NASA TECHNICAL NOTE

NASA TN D-6907

NASA TN D-6907
c.1

TURBULENT BOUNDARY-LAYER VELOCITY PROFILES ON A NONADIABATIC FLAT PLATE AT MACH NUMBER 6.5

by Earl R. Keener and Edward J. Hopkins

Ames Research Center
Moffett Field, Calif. 94035

NATIONAL AERONAUTICS AND SPACE ADMINISTRATION • WASHINGTON, D. C. • AUGUST 1972

1. Report No.	2. Government Accession No.	3. Recipient's Catalog No.
NASA TN D-6907		

4. Title and Subtitle	5. Report Date
TURBULENT BOUNDARY-LAYER VELOCITY PROFILES ON A NONADIABATIC FLAT PLATE AT MACH NUMBER 6.5	August 1972
	6. Performing Organization Code

7. Author(s)	8. Performing Organization Report No.
Earl R. Keener and Edward J. Hopkins	A-4240
	10. Work Unit No.
9. Performing Organization Name and Address	136-13-01-03-00-21
NASA Ames Research Center Moffett Field, Calif. 94305	11. Contract or Grant No.
	13. Type of Report and Period Covered
12. Sponsoring Agency Name and Address	Technical Note
National Aeronautics and Space Administration Washington, D.C. 20546	14. Sponsoring Agency Code

15. Supplementary Notes

16. Abstract

Velocity profiles were obtained from pitot-pressure and total-temperature measurements within a turbulent boundary layer on a large sharp-edged flat plate. Momentum-thickness Reynolds number ranged from 2590 to 8860 and wall-to-adiabatic-wall temperature ratios ranged from 0.3 to 0.5. Measurements were made both with and without boundary layer trips.

Five methods are evaluated for correlating the measured velocity profiles with the incompressible law-of-the-wall and the velocity defect law. The mixing-length generalization of Van Driest gives the best correlation.

17. Key Words (Suggested by Author(s))	18. Distribution Statement
Turbulent Boundary Layer Hypersonic Velocity Profiles Flat Plate Experiment and Theory	Unclassified – Unlimited

19. Security Classif. (of this report)	20. Security Classif. (of this page)	21. No. of Pages	22. Price*
Unclassified	Unclassified	48	$3.00

* For sale by the National Technical Information Service, Springfield, Virginia 22151

NOTATION

A, B constants used in the Van Driest formulas for the velocity-profile transformation, see table 1

C_f local skin friction coefficient

l length of plate

M Mach number

n velocity-profile power-law exponent defined by $\frac{U}{U_e} = \left(\frac{y}{\delta}\right)^{1/n}$

p pressure

Pr Prandtl number

q dynamic pressure, $\frac{1}{2}\rho U^2$

r turbulent temperature recovery factor, $\frac{T_{aw} - T_e}{T_{t,e} - T_e} = 0.88$

$R_{x,tr}$ Reynolds number based on x_{tr}, $\frac{U_e}{\nu_e} x_{tr}$

R_θ Reynolds number based on momentum thickness, $\frac{U_e}{\nu_e}\theta$

T temperature

U velocity component parallel to surface

U_τ friction velocity, $\sqrt{\frac{\tau_w}{\rho}}$

x_{tr} distance from leading edge to transition point indicated by sublimation and heat transfer (peak heating) measurements

y distance normal to flat plate

y_{max} largest height (y) in table 2

δ_n boundary-layer thickness determined by extrapolating to $\frac{U}{U_e} = 1.0$ the measured velocity profile in power-law form, log $\frac{U}{U_e}$ vs log y

δ_p boundary-layer thickness determined by linear extrapolation of pitot-pressure profiles to $\frac{p_{t,2}}{(p_{t,2})_e} = 1.0$

δ_u boundary-layer thickness where $\frac{U}{U_e} = 0.99$

δ^* boundary-layer displacement thickness, $\int_o^{y_{max}} \left(1 - \frac{\rho U}{\rho_e U_e}\right) dy$

θ boundary-layer momentum thickness, $\int_o^{y_{max}} \frac{\rho U}{\rho_e U_e} \left(1 - \frac{U}{U_e}\right) dy$

ϵ ( ) incremental uncertainty in quantity ( )

μ dynamic viscosity from Keyes' formula, see table 1

ν kinematic viscosity

ρ mass density

σ scaling parameter in Baronti-Libby transformation method, see table 1

τ local shear stress

Subscripts

aw adiabatic-wall conditions

B Baronti and Libby

C Coles

e boundary-layer-edge conditions

f edge of boundary-layer sublayer in Coles' transformation method, see table 1

i indicated

o reservoir conditions

t total conditions (isentropic stagnation)

w wall conditions (surface)

2 conditions just downstream of a normal shock wave

Superscripts

$\overline{(\ )}$	incompressible (variable transformed to equivalent constant properties case)
$(\ )'$	reference conditions

TURBULENT BOUNDARY-LAYER VELOCITY PROFILES ON A NONADIABATIC FLAT PLATE AT MACH NUMBER 6.5

Earl R. Keener and Edward J. Hopkins
Ames Research Center

SUMMARY

Velocity profiles were obtained from pitot-pressure and total-temperature measurements within a turbulent boundary layer at one station on a large, nonadiabatic, sharp-edged flat plate at a local Mach number near 6.5. Local skin friction was also directly measured. Momentum-thickness Reynolds numbers ranged from 2590 to 8860 and wall-to-adiabatic-wall temperature ratios ranged from 0.3 to 0.5. Measurements were made both with and without boundary-layer trips.

Five methods are evaluated for correlating the measured velocity profiles with the incompressible form of the law-of-the-wall and the velocity defect law. The mixing-length generalization of Van Driest gives the best correlation.

INTRODUCTION

Several investigations have been conducted at Ames Research Center to obtain measurements of skin-friction, heat transfer, and velocity profiles on flat plates and wind tunnel walls at hypersonic, nonadiabatic wall conditions. The purpose of the investigations has been to use the data to evaluate existing methods of prediction on flat plates. Correlations between the data and methods for predicting skin friction and heat transfer have been reported in references 1 to 5.

This report presents an analysis of the measurements of velocity profiles in a turbulent boundary layer on the large flat plate model used in the investigation of turbulent skin friction, reported in reference 2. Local edge Mach number was about 6.5, momentum-thickness Reynolds number ranged from 2590 to 8860 and wall-to-adiabatic-wall temperature ratios ranged from 0.3 to 0.5. Measurements were made both with and without boundary-layer trips. The experimental velocity profiles are used to evaluate five velocity-profile correlation methods. Two of the methods are reference-temperature methods, T-wall and T' (ref. 6); the other three methods are those of Coles (ref. 7), Baronti and Libby (ref. 8), and Van Driest (ref. 9).

EXPERIMENT

Wind Tunnel

This investigation was conducted in air in the Ames 3.5-Foot Hypersonic Wind Tunnel, in which cold air was passed through an alumina storage heater system and heated to stagnation temperatures ranging from 684° to 1089° K. The Mach 7.4 contoured nozzle was used. Stagnation pressure was varied from 39 to 66 atm and the testing time was between 2 and 3 minutes depending on the pressure level.

Model and Instrumentation

The model was a sharp-edged flat plate, 122.0 cm long, 45.7 cm wide, and 2.5 cm thick, firmly supported by a massive undercarriage instrument housing rigidly attached to the strut of the sting support system (fig. 1(a)). A dimensional sketch of the flat plate is presented in figure 1(b). The boundary layer was surveyed from above the plate at a station 99.6 cm behind the leading edge using a movable survey complex having pitot-pressure, static-pressure, and total-temperature probes (fig. 2). The total-temperature probe was a thermocouple surrounded by a single shield vented at the top behind the thermocouple. A single shield was used because it could be made small and, thereby, minimize possible interference effects from interaction of the probe shock and the boundary layer. Skin friction was measured by a floating-element balance (fig. 3). (See ref. 2 for additional details.) Surface pressures and temperatures were measured along the model centerline. Wind-tunnel total pressure and total temperature were measured in the tunnel reservoir.

Test Conditions

The sharp-edged flat plate was mounted with its test surface 3° to the windward. (This angle was required for another investigation and could not be varied.) The resulting local edge Mach number was about 6.5 for a free-stream Mach number of 7.4. Local unit Reynolds number was varied from about 5 to 13 million per meter by varying tunnel reservoir pressure. Wall-to-adiabatic-wall temperature ratio was varied from 0.3 to 0.5 by varying tunnel reservoir temperature. Nearly isothermal wall conditions (within 30° K) existed along the centerline of the plate as verified by thermocouple measurements. The increase in surface temperature during a run was less than 5 percent of the total temperature. Measurements were made with and without boundary-layer trips.

DATA REDUCTION

Local flow conditions at the edge of the boundary layer on the flat plate (99.6 cm behind the leading edge) were calculated from the measured surface static pressure (p_w), boundary-layer-edge pitot pressure $(p_{t,2})_e$, and the reservoir total temperature $(T_{t,o})$. The compressible flow relations in reference 10 were used in the calculations, which included corrections for calorically

imperfect gas effects as functions of total temperature. Keyes' formula (ref. 11) was used for viscosity. The boundary-layer velocity profiles were calculated from the measured pitot and surface-static pressures (assuming that $p = p_w$) and from an assumed linear variation of total temperature with velocity (i.e., $U/U_e = (T_t - T_w)/(T_{t,e} - T_w)$), which is identical to the well-known Crocco temperature distribution for Prandtl number of unity. Calculated, rather than measured, total temperatures were used because measured T_t was not available for all of the data; however, where available, the measured T_t agreed closely with the calculated temperature distribution (as shown in the discussion section). Additional details of the data reduction procedures are given in reference 2.

Six velocity profiles were selected from the available test conditions (ref. 2) using the criteria of turbulent flow as indicated by the skin friction results, and constant $p_{t,o}$ within 2 N/cm^2 during each boundary-layer survey. Calculated results are tabulated in table 2.

ACCURACY

The estimated probable uncertainties of the recorded and calculated quantities were determined in reference 2 and are given below:

M_e	±3 percent
$(p_{t,2})_e$, q_e, T_w	±2 percent
p_e, $T_{t,e}$, δ^*, θ, τ_w	±5 percent
R_θ	±8 percent
y	±0.013 cm
$\frac{U}{U_e}$	±2 percent

VELOCITY-PROFILE CORRELATION METHODS

Five correlation methods were selected for evaluation. Each method contains functions for correlating compressible velocity profiles with a generalized incompressible profile. Correlation functions for each method are presented in table 1 on the basis of the law-of-the-wall,

$$\frac{\overline{U}}{\overline{U}_\tau} = f\left(\frac{\overline{U}_\tau \overline{y}}{\overline{\nu}}\right)$$

and the velocity defect law

$$\frac{\overline{U}-\overline{U}_e}{\overline{U}_\tau}=f\left(\frac{\overline{y}}{\overline{\delta}}\right)$$

Two of the methods (T-wall and T′ (ref. 6)) follow a reference-temperature approach that was originally developed for the correlation of compressible skin friction. Two methods (Coles, ref. 7, and Baronti and Libby, ref. 8) follow a corresponding-stations approach developed for the transformation of the complete compressible turbulent boundary layer to a corresponding incompressible boundary layer. The last method (Van Driest (ref. 9)) uses the mixing-length approach developed for the correlation of compressible skin friction. (Use of either the Prandtl mixing length (ref. 9) or the Von Kármán mixing length (ref. 12) results in identical functions for eqs. (25) and (29) of table 1.)

RESULTS AND DISCUSSION

Before presenting the analysis of the velocity profiles, several other measurements pertinent to the analysis are discussed. These are skin friction, transition location, surface pressures, and the total-temperature and pitot-pressure surveys.

Local Skin Friction

Local skin friction (surface shear stress) appears as a parameter in all of the correlation formulas for the velocity profiles (table 1). Since measured (rather than theoretical) skin friction is used in this analysis, the measured skin-friction coefficients from reference 2 are again presented in figure 4 as a function of the measured momentum-thickness Reynolds number. The solid symbols correspond to the six boundary-layer profiles in table 2. The cross-hatched bands represent the skin friction by the theory of Van Driest (II)[1] (ref. 12). The band width represents the effect of the experimental range of T_w/T_{aw}. The dashed curve represents the expected level of the data for laminar flow according to the theory of Rubesin and Johnson (ref. 13).

It was a conclusion of reference 2 that the theories of Van Driest (II) (ref. 12) and of Coles (ref. 7—not shown in fig. 4) give the best predictions of skin friction for turbulent flow over a flat plate for these test conditions.

Boundary-Layer Transition

The sublimation technique was used to determine the distance from the leading edge of the plate to the end of transition to verify that turbulent flow existed at the measuring station. The transition Reynolds numbers for natural transition found by using this technique are presented in

[1]The (II) refers to the second skin-friction theory of Van Driest (1954, ref. 12), which uses the Von Karman mixing length in the Prandtl shear-stress; the Van Driest (I) theory (ref. 9) uses the Prandtl mixing length.

figure 5 as a function of unit Reynolds number. The sublimation results show that $R_{x,tr}$ appears to increase with unit Reynolds number (so-called "unit Reynolds number" effect) much the same as the prediction for the end of transition by the semiempirical method of Deem and Murphy (refs. 14 and 15) for 0.013 cm leading-edge thickness. Figure 5 also shows that the sublimation results generally correlate with transition Reynolds numbers determined from peak heating measurements obtained on a heat-transfer flat-plate model of the same size tested in the same facility (data of T. E. Polek, unpublished).

Surface Pressure Distributions

Figure 6 presents the measured surface pressures along the centerline of the model for the conditions of boundary-layer trips off and trips on. Location of the survey station ($x/l = 0.817$) is shown by an arrow. The pressure ranged from 0.20 to as low as 0.063 N/cm^2. (The estimated probable error, $ep_w \simeq \pm 0.0048$ N/cm^2 is indicated on the figure for comparison.) The pressures are not as uniform as expected for a flat plate and the largest variation in surface pressure occurred for the highest surface pressure with boundary-layer trips on. Calculated inviscid pressures for a two-dimensional flow-deflection angle of 3° and $M_\infty = 7.37$ (solid points plotted at the survey station) are generally within experimental accuracy of the measured pressures near the survey station.

Boundary-Layer Total-Temperature Profiles

The total-temperature probe (fig. 2) was calibrated from measurements of the probe outside of the boundary layer where the correct total temperature was taken to be that measured in the reservoir ($T_{t,o}$). The calibration followed a method similar to that used by Winkler (ref. 16) in which the temperature recovery factor $(T_{t,i} - T_e)/(T_t - T_e)$ was shown to correlate with a parameter based on the Nusselt number of the stagnated flow inside the probe and to be independent of Mach number. Winkler's correlating parameter was rewritten as $(p_{t,2})(T_t)^{-7/4}$ and in figure 7 the calibration data are shown as a function of this parameter. Measurements were obtained over a sufficient range of tunnel total pressure to cover the range of flow conditions within the boundary-layer survey, as shown by the arrows. The calibration data at $(p_{t,2})(T_t)^{-7/4} \gtrsim 6\times10^{-6}$ were different for the two free-stream total-temperature levels of 780° and 1050° K.

Boundary-layer total-temperature profiles measured for three of the six velocity profiles presented (table 2(a), (b) and (d)) are shown in figure 8. Static temperatures calculated from T_t and M are presented as T/T_e. The measured temperatures agree well with the calculated Crocco temperatures for each data point (using the linear relationship, written as a function of T_w and M, see ref. 2). The linear relationship is further verified in figure 9 for the conditions shown for a nonadiabatic flat plate.

Boundary-Layer Pitot-Pressure Profiles

The six pitot-pressure profiles from table 2 are presented in figure 10. Three profiles are for natural transition and three are for forced transition using boundary-layer trips. Results show that

the trips cause thickening of the boundary layer. The figure also shows one method of determining a turbulent boundary-layer thickness, obtained by linear extrapolation of the pitot-pressure profiles. The resulting values of δ_p, shown by the arrows, are recorded in table 2.

Boundary-Layer Velocity Profiles

The boundary-layer velocity profiles are presented in figure 11. There are no obvious probe-interference effects near the wall and all profiles are typical of well developed turbulent profiles. The boundary-layer thickness (δ_u), where the value of $U/U_e = 0.99$, is shown by the tick marks and recorded in table 2.

Figure 12 presents a log-log plot of y vs (U/U_e) for the velocity profiles of figure 11 to test the power-law relationship.

$$\frac{U}{U_e} = f(y)^{1/n}$$

The data follow the linear power-law fairings quite closely from $U/U_e = 1.0$ to the data point closest to the wall. The boundary-layer thickness (δ_n), determined from the intersection of the power-law fairing with $U/U_e = 1.0$, is shown by the arrows and the values are recorded in table 2.

In figure 13 the velocity-profile power-law exponent is presented as a function of Reynolds number R_θ. Included is an adiabatic-wall curve (Fenter, ref. 17) that approximately represents existing experimental results for subsonic and supersonic Mach number. (Fenter's analysis indicated that the power-law factor is not a function of Mach number.) These results clearly do not follow the trend with Reynolds number of Fenter's curve. Instead, the value of n is about double that of the subsonic/supersonic value of about 5 at $R_\theta \simeq 2500$ and approaches the subsonic/supersonic value of about 7 at $R_\theta \simeq 10^4$. Recently, Johnson and Bushnell (ref. 18) summarized a large number of existing measurements, including the present results, and reported that the power-law exponents at $M > 4$ are often as high as 10 or more (termed overshoot) in the low Reynolds number range for flat plates, cones, and hollow cylinders but that data from wind-tunnel walls often do not show this effect.

Results from four other investigations are also shown in figure 13. Boundary-layer measurements on the walls of the Ames 3.5-Foot Hypersonic Wind Tunnel at $M_e = 7.4$ (ref. 19) and the Ames 8- by 7-Foot Supersonic Wind Tunnel (unpublished) are represented by two identified lines, which lie within 10 percent of Fenter's empirical curve. (Skin-friction measurements from the wall tests were reported in refs. 2, 19, and 20). Results from the Naval Ordinance Laboratory boundary-layer channel at $M = 5$ (ref. 21) are represented by another line, which also lies within 10 percent of the Fenter curve, although at a slightly different slope. A wind-tunnel wall measurement by Hill (ref. 22) at $M = 9$ and low Reynolds number $(R_\theta = 2000)$ lies on Fenter's curve. Finally, the cross-hatched area represents a more recent investigation (ref. 3) extending the results to $R_\theta \simeq 1.8 \times 10^4$ using a flat plate that was very similar to that used in the present investigation. The power-law exponent appears to follow close to the subsonic/supersonic variation for $R_\theta \gtrsim 7 \times 10^3$.

Boundary-Layer Thickness

The edge of a turbulent boundary layer is difficult to determine accurately from experimental profiles. Neither δ^* nor θ require an accurate value for δ. However, the velocity-defect correlations require a more accurate determination of boundary-layer thickness. Three methods for determining δ have been described in the discussion of the pitot-pressure profiles (δ_p), the velocity profiles (δ_u), and the power-law exponent (δ_n). Tabulated results from table 2 show that δ_u is close to δ_n whereas δ_p is usually much larger. The power-law method was chosen for use in the equations for $\bar{y}/\bar{\delta}$ in table 1 because this method gives consistent and rational values and because the power law is a characteristic expression for the outer part of the velocity profile.

Velocity-Profile Correlation Methods

The five velocity-profile correlation methods given in table 1 were selected for evaluation using the velocity profiles listed in table 2. The transformed velocity profiles are compared in figures 14 to 19 on the basis of the law-of-the-wall and the velocity-defect law, which have been shown to correlate incompressible profiles. Each method is evaluated by observing how well the compressible (variable-density) velocity profiles are transformed to an incompressible (constant-density) profile. Coles' incompressible listing (table 3), determined empirically (ref. 23), is used in this analysis to represent the incompressible profiles.

The deviation of the transformed profiles from Coles' curve for the law-of-the-wall can be expressed in terms of an equivalent percentage deviation in skin friction (τ_w), which appears in the correlating parameters. The data were transformed using measured τ_w rather than the theoretical τ_w that would be obtained from the comparable skin-friction law for $C_f = f(R_\theta)$ for each method (ref. 2). On the other hand, a value of τ_w could have been chosen that would have forced the data to agree with Coles' incompressible law-of-the-wall curve, and the resulting τ_w could have been compared to the measured value. The latter method, known as the Clauser technique for obtaining skin friction from velocity profiles, is described in reference 24. For discussions of previous analyses of incompressible and compressible velocity profile results, see references 25 and 26.

Figures 14 to 18 show the results of using the five correlation methods on three of the six measured velocity profiles, one at each temperature ratio tested (T_w/T_{aw} = 0.32, 0.43, and 0.51), obtained with boundary-layer trips on.

T-wall method— The simplest correlation method is the wall reference-temperature method. This method is of interest because it has been used successfully to correlate the effect of compressibility on laminar skin friction and velocity profiles for adiabatic flat plates at Mach numbers up to 5. It is readily apparent in figure 14 that the T-wall method does not correlate the data since the three profiles do not collapse to a single curve in the law-of-the-wall transformation. The velocity-defect transformation does not correlate any of the profiles with the incompressible curve.

T' method– Another simple correlation method is to evaluate the local fluid properties at a T' reference temperature, similar to the reference-temperature correlations for skin friction. The T' method was first shown by Rubesin and Johnson (ref. 13) to extend the correlation of laminar

skin friction to Mach numbers much higher than 5. The reference temperature expression (eq. (6)) of Sommer and Short (ref. 6) was chosen to represent this type of transformation. Figure 15 shows that the T' method correlates the law-of-the-wall profiles better than the T-wall method. Expressed in terms of skin friction (τ_w), the transformed profiles are within 8 percent of Coles' incompressible curve. For example, an 8 percent higher τ_w than that measured would put the data for $T_w/T_{aw} = 0.32$ and 0.43 onto Coles' curve. Again, none of the velocity-defect profiles are correlated with the incompressible curve.

Method of Coles (ref. 7)— Figure 16 presents the results of the transformation of Coles', developed from his law of corresponding stations. The transformed profiles lie parallel to the incompressible law-of-the-wall curve but are displaced as much as 13 percent in τ_w. It is interesting to note, however, that Coles' skin-friction equation (ref. 2) predicts the measured skin friction within 5 percent Evidently, the skin friction predicted by the transformation functions for skin friction can be different from the skin friction obtained from the velocity profiles using the functions derived from the same method. Correlation of the velocity-defect profiles with the incompressible curve is poor.

Method of Baronti and Libby (ref. 8)— In figure 17 the results are presented for the transformation of Baronti and Libby, which is an extension of Coles' method. The method correlates the effect of temperature by collapsing the law-of-the-wall profiles; however, the transformed profiles have a different slope than the incompressible curve. These transformed profiles are similar to those shown by Baronti and Libby at high supersonic Mach numbers and by Bertram *et al.* (ref. 25) and at hypersonic Mach numbers by Watson and Cary (ref. 26). Skin friction can be obtained from the velocity profiles within 10 percent of the measured values if an abscissa $(\bar{U}_\tau \bar{y}/\bar{\nu})$ of about 200 is used to correlate with Coles' curve. Correlation of the velocity-defect profiles with the incompressible curve is very poor; a similar result with this method was reported in reference 8.

Method of Van Driest (ref. 9)— The final correlation method considered (fig. 18) is that of Van Driest, developed from mixing-length theory. The method gives the best correlation of the law-of-the-wall profiles (within 5 percent of Coles' incompressible curve). In addition, it is the only method that transforms the velocity-defect profiles close to the incompressible curve. Similar results are obtained (fig. 19) with the Van Driest method using the three velocity profiles in table 2 with boundary-layer trips off (natural transition). The velocity-defect transformation shows an effect of Reynolds number in both figures 18 and 19. The correlation deteriorates with decreasing Reynolds number; however, this agrees with the power-law-exponent overshoot at the lower Reynolds numbers (fig. 13). The correlations of the Van Driest law-of-the-wall transformations at all Reynolds numbers presented are compatible with the correlation of skin friction (fig. 4) for the Van Driest method. The correlations indicate that skin friction can also be determined from experimental velocity profiles (Clauser technique) within ±5 percent.

The results of figures 18 and 19 confirm that the mixing-length concept can be used to analyze some of the characteristics of compressible turbulent boundary layers at Mach numbers up to at least 7. For example, Maise and McDonald (ref. 27) chose the Van Driest generalized velocity distribution to calculate the effect of compressibility on the shear-stress, mixing-length, and eddy-viscosity distributions at Mach numbers up to 5. Mathews, Childs, and Paynter (ref. 28) used the Van Driest generalization in Coles' universal wall-wake equation to calculate velocity profiles for cases with pressure gradient and shock-wave boundary-layer interaction.

CONCLUDING REMARKS

Velocity profiles were obtained from pitot-pressure and total-temperature measurements within a turbulent boundary layer at one station on a large (1.22 m length) nonadiabatic, sharp-edged flat plate at a local Mach number near 6.5. Local skin friction was also directly measured. Momentum thickness Reynolds numbers ranged from 2590 to 8860 and wall-to-adiabatic-wall temperature ratios ranged from 0.3 to 0.5. Measurements were made both with and without boundary-layer trips.

The sublimation technique was used to determine the location of transition. The results generally correlate with the location of peak heating. Measured total temperatures in the boundary layer follow the Crocco linear variation with velocity. Boundary-layer trips produce no obvious distortion effects on the velocity profiles. The velocity-profile power-law exponent does not follow the normal subsonic/supersonic trend of increasing with increasing Reynolds number. Instead, the exponent is about double the subsonic/supersonic value of about 5 at low Reynolds numbers near peak skin friction ($R_\theta \simeq 2500$) and approaches the subsonic/supersonic value of about 7 at a momentum-thickness Reynolds number of about 10^4.

Five methods are evaluated for correlating the measured velocity profiles with the incompressible form of the law-of-the-wall and the velocity defect law. The Van Driest method gives the best correlation for both the law-of-the-wall and the velocity-defect law. Law-of-the-wall transformations are satisfactory at all Reynolds numbers presented, which agrees with the good correlation of skin friction reported previously for the Van Driest method (ref. 2). This result indicates that skin friction can be determined from experimental velocity profiles (Clauser technique) within ±5 percent, using the Van Driest law-of-the-wall transformation. The velocity-defect profiles correlate approximately with the incompressible profile at the highest momentum-thickness Reynolds numbers near 8000. The correlation deteriorates with decreasing Reynolds number, a result that agrees with the power-law-exponent results.

Ames Research Center
National Aeronautics and Space Administration
Moffett Field, California, 94035, March 23, 1972

REFERENCES

1. Hopkins, Edward J.; Rubesin, Morris W.; Inouye, Mamoru; Keener, Earl R.; Mateer, George C.; and Polek, Thomas E.: Summary and Correlation of Skin-Friction and Heat-Transfer Data for a Hypersonic Turbulent Boundary Layer on Simple Shapes. NASA TN D-5089, 1969.

2. Hopkins, Edward J.; Keener, Earl R.; and Louie, Pearl T.: Direct Measurements of Turbulent Skin Friction on a Nonadiabatic Flat Plate at Mach Number 6.5 and Comparisons with Eight Theories. NASA TN D-5675, 1970.

3. Hopkins, Edward J.; Keener, Earl R.; Polek, Thomas E.; and Dwyer, Harry A.: Hypersonic Turbulent Skin Friction and Boundary-Layer Profiles Measured on Nonadiabatic Flat Plates. AIAA J., vol. 10, no.1, Jan. 1972, p. 40.

4. Hopkins, Edward J.; and Keener, Earl R.: Unit Reynolds Number Effects on Boundary-Layer Transition at Mach 6. AIAA J., vol. 6, no. 5, May 1968, p. 956.

5. Keener, Earl R.; and Hopkins, Edward J.: Use of Preston Tubes for Measuring Hypersonic Turbulent Skin Friction. NASA TN D-5544, 1969.

6. Sommer, Simon C.; and Short, Barbara J.: Free-Flight Measurements of Turbulent Boundary-Layer Skin Friction in the Presence of Severe Aerodynamic Heating at Mach Numbers from 2.8 to 7.0. NACA TN 3391, 1955 (also IAS J., vol. 23, no. 6, June 1956, pp. 536-542).

7. Coles, Donald E.: The Turbulent Boundary Layer in a Compressible Fluid. Phys. Fluids, vol. 7, no. 9, Sept. 1964, pp. 1403-1423 (also RAND Rep. R-403-PR, 1962).

8. Baronti, Paolo O.; and Libby, Paul A.: Velocity Profiles in Turbulent Compressible Boundary Layers. AIAA J. vol. 4, no. 2, Feb. 1966, pp. 193-202.

9. Van Driest, Edward R.: Turbulent Boundary Layer in Compressible Fluids. IAS J., vol. 18, no. 3, March 1951, pp. 145-160, 216.

10. Ames Research Staff: Equations, Tables, and Charts for Compressible Flow. NACA Rep. 1135, 1953.

11. Bertram, Mitchel H.: Comment on "Viscosity of Air." J. Spacecraft and Rockets, vol. 4, no. 2, Feb. 1967, p. 287.

12. Van Driest, E. R.: The Problem of Aerodynamic Heating. Aeron. Eng. Rev., vol. 15, no. 10, Oct. 1956, pp. 26-41.

13. Rubesin, Morris W.; and Johnson, H. A.: A Critical Review of Skin-Friction and Heat-Transfer Solutions of the Laminar Boundary Layer of a Flat Plate. Trans. ASME, vol. 71, no. 4, May 1949, pp. 383-388.

14. Deem, Ralph E.; and Murphy, James S.: Flat Plate Boundary Layer Transition at Hypersonic Speeds. AIAA Paper 65-128, 1965.

15. Hopkins, Edward J.; Jillie, Don W.; and Sorensen, Virginia L.: Charts for Estimating Boundary-Layer Transition on Flat Plates. NASA TN D-5846, 1970.

16. Winkler, Eva M.: Stagnation Temperature Probes for Use at High Supersonic Speeds and Elevated Temperatures. NAVORD Report 3834, Oct. 1954.

17. Fenter, Felix W.: A New Analytical Method for the Prediction of Turbulent Boundary Layer Characteristics on a Thermally-Insulated Flat Plate at Supersonic Speeds. Report DRL-343, CF-2095, Defense Research Lab., University of Texas, June 1954.

18. Johnson, Charles B.; and Bushnell, Dennis M.: Power-Law Velocity-Profile-Exponent Variations with Reynolds Number, Wall Cooling, and Mach Number in a Turbulent Boundary Layer. NASA TN D-5753, 1970.

19. Hopkins, Edward J.; and Keener, Earl R.: Pressure-Gradient Effects on Hypersonic Turbulent Skin Friction and Boundary-Layer Profiles. AIAA Paper 72-215, 1972.

20. Hopkins, Edward J.; and Keener, Earl R.: Study of Surface Pitots for Measuring Turbulent Skin Friction at Supersonic Mach Numbers – Adiabatic Wall. NASA TN D-3478, 1966.

21. Lee, Roland E.; Yanta, William J.; and Leonas, Annette C.: Velocity Profile, Skin Friction Balance, and Heat Transfer Measurements of the Turbulent Boundary Layer at Mach 5. Proc. 1968 Heat Transfer and Fluid Mechanics Institute, Univ. of Washington, Seattle, June 17, 18, 1968, Stanford Univ. Press, 1968, p. 3-17.

22. Hill, F. K.: Boundary-Layer Measurements in Hypersonic Flow. IAS J., vol. 23, no. 1, Jan. 1956, pp. 35-42.

23. Coles, Donald: Measurements in the Boundary Layer on a Smooth Flat Plate in Supersonic Flow. Part I. The Problem of a Turbulent Boundary Layer. Report 20-69, Jet Propulsion Lab., California Institute of Technology, June 1953.

24. Allen, Jerry M.: Use of Baronti-Libby Transformation and Preston Tube Calibrations to Determine Skin Friction from Turbulent Velocity Profiles. NASA TN D-4853, 1968.

25. Bertram, Mitchel H.; Cary, Aubrey M., Jr.; and Whitehead, Allen H., Jr.: Experiments with Hypersonic Turbulent Boundary Layers on Flat Plates and Delta Wings. AGARD Specialists' Meeting on Hypersonic Boundary Layers and Flow Fields, London, England, May 1-3, 1968. AGARD CP-30.

26. Watson, Ralph D.; and Cary, Aubrey M., Jr.: Transformation of Hypersonic Turbulent Boundary Layers to Incompressible Form. AIAA J., vol. 5, no. 6, June 1967, pp. 1202-3.

27. Maise, George; and McDonald, Henry: Mixing Length and Kinematic Eddy Viscosity in a Compressible Boundary Layer. AIAA J., vol. 6, no. 1, Jan. 1968, pp. 73-80.

28. Mathews, Douglas C.; Childs, Morris E.; and Paynter, Gerald C.: Use of Coles' Universal Wake Function for Compressible Turbulent Boundary Layers. J. Aircraft, vol. 7, no. 2, March-April 1970, pp. 137-140.

TABLE 1.– TRANSFORMATION FUNCTIONS FOR VELOCITY PROFILES

	Wall reference temperature		T' reference temperature		Coles (ref. 7)		Baronti and Libby (ref. 8)		Van Driest (ref. 9)	
					$\dfrac{U/U_e}{\sqrt{\bar{C}_{f,C}/2}}$ (10) where $\bar{C}_{f,C} = \dfrac{\rho_e \mu_e}{\rho_w \mu_w} \dfrac{\bar{\mu}}{a\mu_e} C_f$ (11); $\dfrac{\bar{\mu}}{a\mu_e} = \dfrac{\mu_C}{\mu_e}$ (12); $T_C = \dfrac{T_e}{430} \int_0^{430} \left(\dfrac{T}{T_e}\right) d\left(\dfrac{\bar{U}_\tau \bar{y}}{\bar{\nu}}\right)$ (13); $\dfrac{T}{T_e} = \dfrac{T_w}{T_e} + \left(1 + 0.2M_e^2 - \dfrac{T_w}{T_e}\right)\left(\dfrac{\bar{U}}{\bar{U}_\tau}\right)\sqrt{\dfrac{\bar{C}_{f,C}}{2}} - \left(\dfrac{\bar{U}}{\bar{U}_\tau}\right)^2 \dfrac{0.2M_e^2\left(\bar{C}_{f,C}\right)}{2}$ (14)		$\dfrac{U/U_e}{\sqrt{\bar{C}_{f,BL}/2}}$ (18) where $\bar{C}_{f,BL} = \dfrac{\rho_e \mu_e}{\rho_w \mu_w} \dfrac{\bar{\mu}}{a\mu_e} C_f$ (19); $\dfrac{a\mu_e}{\bar{\mu}} = \dfrac{\rho_f}{\rho_e} \dfrac{\mu_e}{\mu_f} \left[\dfrac{T_w}{T_e} + \left(1 + 0.2M_e^2 - \dfrac{T_w}{T_e}\right) \times \sqrt{\dfrac{\bar{C}_{f,BL}}{2}}(10.6) - 0.2M_e^2 \dfrac{\bar{C}_{f,BL}}{2}(10.6)^2\right]$ (20); $T_f = T_e\left[\left(\dfrac{T_w}{T_e}\right) + \left(1 + 0.2M_e^2 - \dfrac{T_w}{T_e}\right)\sqrt{\dfrac{\bar{C}_{f,BL}}{2}}(10.6) - 0.2M_e^2 \dfrac{\bar{C}_{f,BL}}{2}(10.6)^2\right]$ (21)		
					$\bar{U}/\bar{U}_\tau$ given as a function of $\bar{U}_\tau \bar{y}/\bar{\nu}$ in table 3 (taken from ref. 23) equation (14) is based on a Crocco temperature distribution for unit Prandtl number. $\bar{C}_{f,C}$ is obtained from equations (11) to (14) by iteration.		$\bar{C}_{f,BL}$ is obtained from eqs. (19) through (21) by iteration.			
$\dfrac{\bar{U}_\tau \bar{y}}{\bar{\nu}}$	$\dfrac{U_e}{\nu_w}\left(\sqrt{\dfrac{C_f}{2}}\dfrac{T_w}{T_e}\right)y$	(2)	$\dfrac{U_e}{\nu'}\left(\sqrt{\dfrac{C_f}{2}}\dfrac{T}{T_e}\right)y$	(7)	$\dfrac{U_e}{\nu_e}\sqrt{\dfrac{\bar{C}_{f,C}}{2}}\dfrac{a\mu_e}{\bar{\mu}}\int_0^y \dfrac{\rho}{\rho_e}\,dy$	(15)	$\dfrac{U_e}{T_e}\sqrt{\dfrac{\bar{C}_{f,BL}}{2}}\dfrac{a\mu_e}{\bar{\mu}}\int_0^y \dfrac{\rho}{\rho_e}\,dy$	(22)	$\dfrac{U_e}{\nu_w}\left(\sqrt{\dfrac{C_f}{2}}\dfrac{T_w}{T_e}\right)y$	(28)
$\dfrac{\bar{U}-\bar{U}_e}{\bar{U}_\tau}$	$\dfrac{\left(U/U_e\right)-1}{\sqrt{\left(C_f/2\right)\left(T_w/T_e\right)}}$	(3)	$\dfrac{\left(U/U_e\right)-1}{\sqrt{\left(C_f/2\right)\left(T'/T_e\right)}}$	(8)	$\dfrac{\left(U/U_e\right)-1}{\sqrt{\bar{C}_{f,C}/2}}$	(16)	$\dfrac{\left(U/U_e\right)-1}{\sqrt{\bar{C}_{f,BL}/2}}$	(23)	$\dfrac{1}{A\sqrt{\left(C_f/2\right)\left(T_w/T_e\right)}}\left\{\sin^{-1}\left[\dfrac{2A^2\left(U/U_e\right)-B}{\sqrt{B^2+4A^2}}\right] - \sin^{-1}\left(\dfrac{2A^2-B}{\sqrt{B^2+4A^2}}\right)\right\}$	(29)
$\dfrac{\bar{y}}{\delta}$	$\dfrac{y}{\delta_n}$	(4)	$\dfrac{y}{\delta_n}$	(9)	$\dfrac{\int_0^y \left(\rho/\rho_e\right)dy}{\int_0^\delta \left(\rho/\rho_e\right)dy}$	(17)	$\dfrac{\int_0^y \left(\rho/\rho_e\right)dy}{\int_0^\delta \left(\rho/\rho_e\right)dy}$	(24)	$\dfrac{y}{\delta_n}$	(30)

NOTE: Experimental values for C_f were used in above functions rather than theoretical values

Keyes' viscosity formula (ref. 11) used in the calculations is

$$\mu = 1.49\times10^{-8}\ \sqrt{T}\left(1 + \frac{122}{T}\times10^{-\frac{5}{T}}\right)^{-1}\ \frac{\text{N-sec}}{\text{m}^2} \qquad (31)$$

T = temperature, °K

TABLE 2.– BOUNDARY-LAYER SURVEYS

(a)

$M_e = 6.21$	$p_{t,\infty} = 394$ N/cm^2
$T_{t,e} = 1028^\circ$ K	$\left(p_{t,2}\right)_e = 5.80$ N/cm^2
$T_w = 324^\circ$ K	$p_e = 0.116$ N/cm^2
$T_e = 123^\circ$ K	$\left(\rho_e U_e/\nu_e\right)\times 10^{-6} = 5.18$ m^{-1}
$T_w/T_{aw} = 0.34$	$U_e = 1383$ m/sec
$\delta_u = 1.02$ cm	$\delta^* = 0.559$ cm
$\delta_p = 1.30$ cm	$\theta = 0.0498$ cm
$\delta_n = 1.12$ cm	$H = 11.2$
$n = 10.9$	$R_\theta = 2{,}590$
Data symbol ○	$C_f = 0.00156$

B.L. trips off

y, cm	M/M_e	T/T_e	U/U_e	$T_t/T_{t,e}$ measured
0.24	0.5651	2.225	0.8429	0.907
.27	.5757	2.179	.8498	.913
.39	.6316	1.950	.8821	.929
.51	.6865	1.753	.9090	.948
.68	.7682	1.501	.9413	.963
.74	.7882	1.447	.9480	.968
1.08	.9245	1.135	.9848	.987
1.26	.9630	1.063	.9929	.987
1.28	.9647	1.060	.9933	.986
1.41	.9807	1.032	.9964	.989
1.68	.9937	1.010	.9988	.995
1.85	.9966	1.006	.9994	.996
2.42	1.0000	1.000	1.0000	1.000

TABLE 2.– BOUNDARY-LAYER SURVEYS – Continued

(b)

$M_e = 6.39$	$p_{t,\infty} = 666$ N/cm^2
$T_{t,e} = 1089^\circ$ K	$\left(p_{t,2}\right)_e = 9.87$ N/cm^2
$T_w = 326^\circ$ K	$p_e = 0.186$ N/cm^2
$T_e = 125^\circ$ K	$\left(\rho_e U_e/\nu_e\right)\times 10^{-6} = 8.43$ m^{-1}
$T_w/T_{aw} = 0.32$	$U_e = 1432$ m/sec
$\delta_u = 1.37$ cm	$\delta^* = 0.698$ cm
$\delta_p = 1.60$ cm	$\theta = 0.0625$ cm
$\delta_n = 1.52$ cm	$H = 11.1$
$n = 7.5$	$R_\theta = 5{,}280$
Data symbol □	$C_f = 0.00122$

B.L. trips on

y, cm	M/M_e	T/T_e	U/U_e	$T_t/T_{t,e}$ measured
0.17	0.4509	2.819	0.7565	0.854
.28	.5071	2.524	.8054	.873
.40	.5480	2.326	.8356	.889
.47	.5918	2.128	.8634	.902
.52	.6122	2.043	.8750	.913
.64	.6620	1.851	.9006	.927
.68	.6792	1.789	.9085	.931
.77	.7147	1.670	.9235	.940
.91	.7626	1.523	.9412	.955
.94	.7789	1.477	.9466	.958
1.01	.8005	1.419	.9534	.963
1.06	.8234	1.360	.9602	.970
1.12	.8478	1.301	.9669	.973
1.25	.8990	1.187	.9796	.985
1.30	.9128	1.159	.9827	.989
1.46	.9550	1.078	.9916	.998
1.78	1.0000	1.000	1.0000	1.000

TABLE 2.– BOUNDARY-LAYER SURVEYS – Continued

(c)

$M_e = 6.42$	$p_{t,\infty} = 385$ N/cm^2
$T_{t,e} = 764^\circ$ K	$\left(p_{t,2}\right)_e = 6.09$ N/cm^2
$T_w = 312^\circ$ K	$p_e = 0.114$ N/cm^2
$T_e = 85^\circ$ K	$\left(\rho_e U_e/\nu_e\right)\times 10^{-6} = 9.12$ m^{-1}
$T_w/T_{aw} = 0.45$	$U_e = 1185$ m/sec
$\delta_u = 1.22$ cm	$\delta^* = 0.658$ cm
$\delta_p = 1.50$ cm	$\theta = 0.0518$ cm
$\delta_n = 1.24$ cm	$H = 12.7$
$n = 9.4$	$R_\theta = 4{,}720$
Data symbol ◇	$C_f = 0.00123$
	B.L. trips off

y, cm	M/M_e	T/T_e	U/U_e
0.21	0.4872	2.749	0.8079
.34	.5471	2.414	.8501
.48	.6073	2.121	.8844
.59	.6600	1.899	.9094
.72	.7192	1.682	.9326
.82	.7640	1.538	.9475
.97	.8198	1.381	.9633
1.09	.8745	1.246	.9764
1.21	.9114	1.166	.9842
1.28	.9334	1.122	.9885
1.48	.9743	1.045	.9958
1.61	.9873	1.022	.9980
1.72	.9936	1.011	.9990
1.81	.9983	1.003	.9997
1.99	1.0000	1.000	1.0000

TABLE 2.– BOUNDARY-LAYER SURVEYS – Continued

(d)

$M_e = 6.42$	$p_{t,\infty} = 232$ N/cm^2
$T_{t,e} = 784^\circ$ K	$\left(p_{t,2}\right)_e = 3.70$ N/cm^2
$T_w = 306^\circ$ K	$p_e = 0.069$ N/cm^2
$T_e = 87^\circ$ K	$\left(\rho_e U_e/\nu_e\right) \times 10^{-6} = 5.34$ m^{-1}
$T_w/T_{aw} = 0.43$	$U_e = 1200$ m/sec
$\delta_u = 1.75$ cm	$\delta^* = 0.919$
$\delta_p = 2.11$ cm	$\theta = 0.0744$
$\delta_n = 1.68$ cm	$H = 12.4$
$n = 8.5$	$R_\theta = 3{,}960$
Data symbol △	$C_f = 0.00125$

B.L. trips on

y, cm	M/M_e	T/T_e	U/U_e	$T_t/T_{t,e}$ measured
0.21	0.4541	2.937	0.7782	0.876
.34	.4954	2.688	.8123	.894
.48	.5418	2.433	.8451	.914
.58	.5809	2.237	.8688	.928
.71	.6245	2.040	.8918	.944
.82	.6594	1.897	.9081	.956
.97	.7043	1.730	.9264	.973
1.17	.7711	1.515	.9491	.990
1.23	.7836	1.478	.9528	.994
1.48	.8513	1.300	.9708	1.006
1.72	.9135	1.161	.9845	1.006
1.82	.9369	1.114	.9890	1.010
2.11	.9770	1.040	.9962	1.006
2.21	.9848	1.026	.9975	1.005
2.67	1.0000	1.000	1.0000	1.000

TABLE 2.– BOUNDARY-LAYER SURVEYS – Continued

(e)

$M_e = 6.50$	$p_{t,\infty} = 452$ N/cm^2
$T_{t,e} = 684^\circ$ K	$\left(p_{t,2}\right)_e = 7.31$ N/cm^2
$T_w = 318^\circ$ K	$p_e = 0.133$ N/cm^2
$T_e = 73^\circ$ K	$\left(\rho_e U_e/\nu_e\right)\times 10^{-6} = 13.4$ m^{-1}
$T_w/T_{aw} = 0.51$	$U_e = 1119$ m/sec
$\delta_u = 1.35$ cm	$\delta^* = 0.704$
$\delta_p = 1.52$ cm	$\theta = 0.0518$
$\delta_n = 1.35$ cm	$H = 13.6$
$n = 8.7$	$R_\theta = 6{,}910$
Data symbol △	$C_f = 0.00106$
	B.L. trips off

y, cm	M/M_e	T/T_e	U/U_e
0.14	0.4208	3.283	0.7624
.28	.4822	2.857	.8149
.40	.5282	2.573	.8472
.55	.6069	2.157	.8914
.64	.6462	1.980	.9093
.76	.7012	1.762	.9308
.89	.7617	1.556	.9502
1.02	.8179	1.393	.9652
1.16	.8827	1.232	.9797
1.25	.9179	1.155	.9865
1.41	.9559	1.079	.9931
1.55	.9777	1.039	.9966
1.63	.9892	1.019	.9984
1.68	.9917	1.014	.9988
1.95	1.0000	1.000	1.0000

TABLE 2.– BOUNDARY-LAYER SURVEYS – Concluded

(f)

$M_e = 6.50$	$p_{t,\infty} = 452$ N/cm^2
$T_{t,e} = 689^\circ$ K	$(p_{t,2})_e = 7.29$ N/cm^2
$T_w = 318^\circ$ K	$p_e = 0.133$ N/cm^2
$T_e = 74^\circ$ K	$(\rho_e U_e/\nu_e) \times 10^{-6} = 13.1$ m^{-1}
$T_w/T_{aw} = 0.51$	$U_e = 1123$ m/sec
$\delta_u = 1.65$ cm	$\delta^* = 0.909$
$\delta_p = 1.85$ cm	$\theta = 0.0676$
$\delta_n = 1.52$ cm	$H = 13.5$
$n = 6.7$	$R_\theta = 8{,}860$
Data symbol $\triangle$	$C_f = 0.00100$

B.L. trips on

y, cm	M/M_e	T/T_e	U/U_e
0.12	0.3696	3.662	0.7072
.25	.4190	3.287	.7598
.36	.4486	3.077	.7867
.51	.5140	2.653	.8371
.60	.5472	2.461	.8584
.74	.5935	2.220	.8841
.86	.6405	2.003	.9064
.98	.6922	1.794	.9271
1.13	.7483	1.598	.9460
1.26	.8054	1.426	.9619
1.37	.8457	1.320	.9716
1.49	.8895	1.216	.9810
1.76	.9646	1.063	.9945
2.25	.9946	1.009	.9992
2.52	1.0000	1.000	1.0000

TABLE 3.– INCOMPRESSIBLE LAW OF THE WALL AND VELOCITY DEFECT LAW VALUES
[from ref. 23]

Law of the wall		Velocity defect law	
$\frac{\bar{U}_\tau \bar{y}}{\bar{\nu}}$	$\frac{\bar{U}}{\bar{U}_\tau}$	$\frac{\bar{y}}{\bar{\delta}}$	$\frac{\bar{U}-\bar{U}_e}{\bar{U}_\tau}$
0	0	0.010	−14.31
1	.99	.015	−13.30
2	1.96	.020	−12.58
3	2.90	.025	−12.02
4	3.80	.030	−11.57
5	4.65	.040	−10.85
6	5.45	.050	−10.29
7	6.19	.060	−9.83
8	6.87	.080	−9.11
9	7.49	.100	−8.56
10	8.05	.150	−7.54
12	9.00	.200	−6.70
14	9.76	.250	−6.00
16	10.40	.300	−5.37
18	10.97	.350	−4.79
20	11.49	.400	−4.25
24	12.34	.450	−3.73
28	12.99	.500	−3.23
32	13.48	.550	−2.76
36	13.88	.600	−2.31
40	14.22	.650	−1.89
44	14.51	.700	−1.50
50	14.87	.750	−1.14
60	15.33	.800	−.82
80	16.04	.850	−.53
100	16.60	.900	−.29
150	17.61	.950	−.10
200	18.33	1.000	0
300	19.34		
400	20.06		
500	20.62		
600	21.08		
800	21.79		
1000	22.35		
1500	23.36		
2000	24.08		
3000	25.09		
4000	25.81		
5000	26.37		
6000	26.83		
8000	27.54		
10000	28.10		

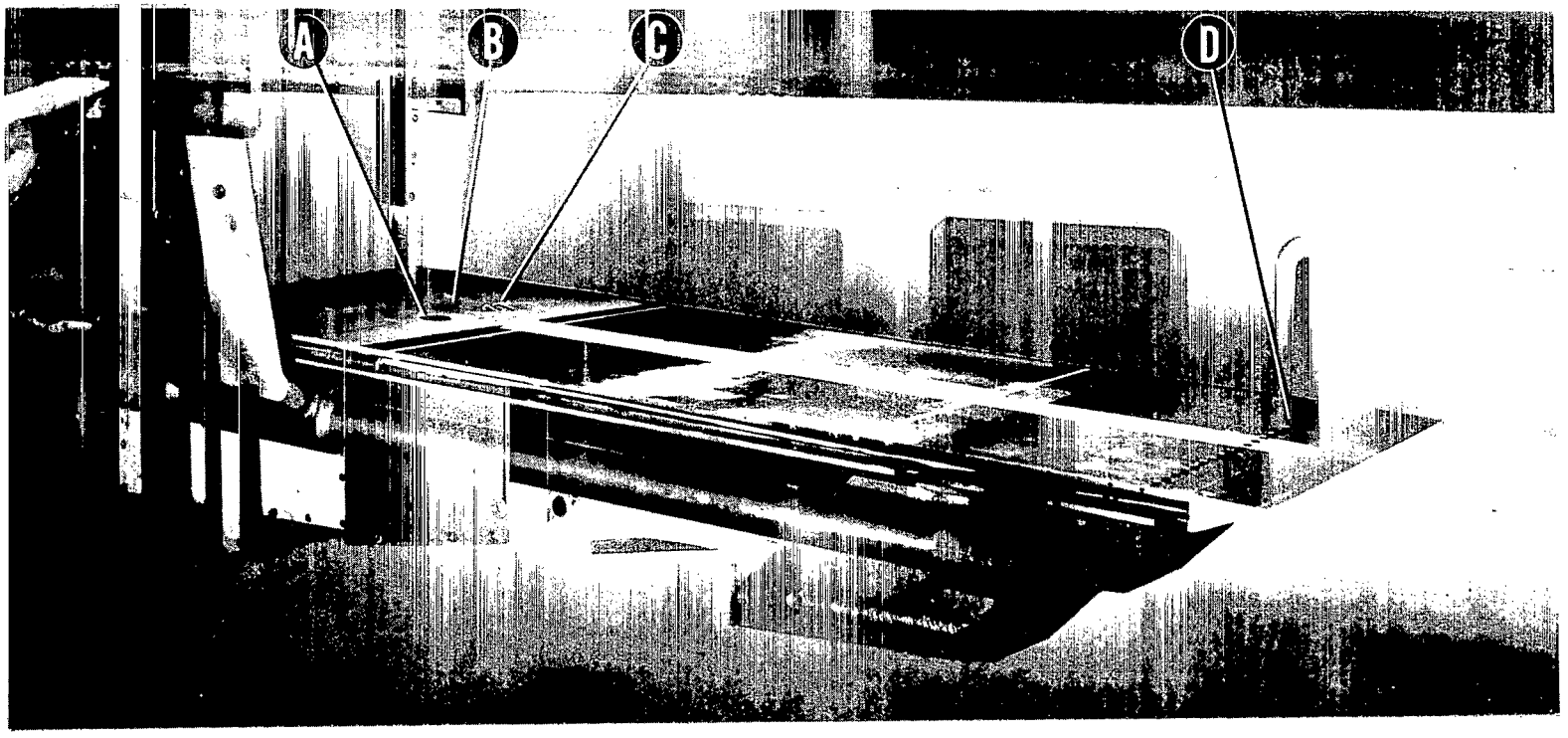

Ⓐ Skin - friction balance
Ⓑ Boundary - layer survey complex
Ⓒ Preston tubes (ref. 5)
Ⓓ Boundary - layer trips

(a) Mounted in the Ames 3.5-Foot Hypersonic Wind Tunnel.

Figure 1.– Sharp-edged flat plate.

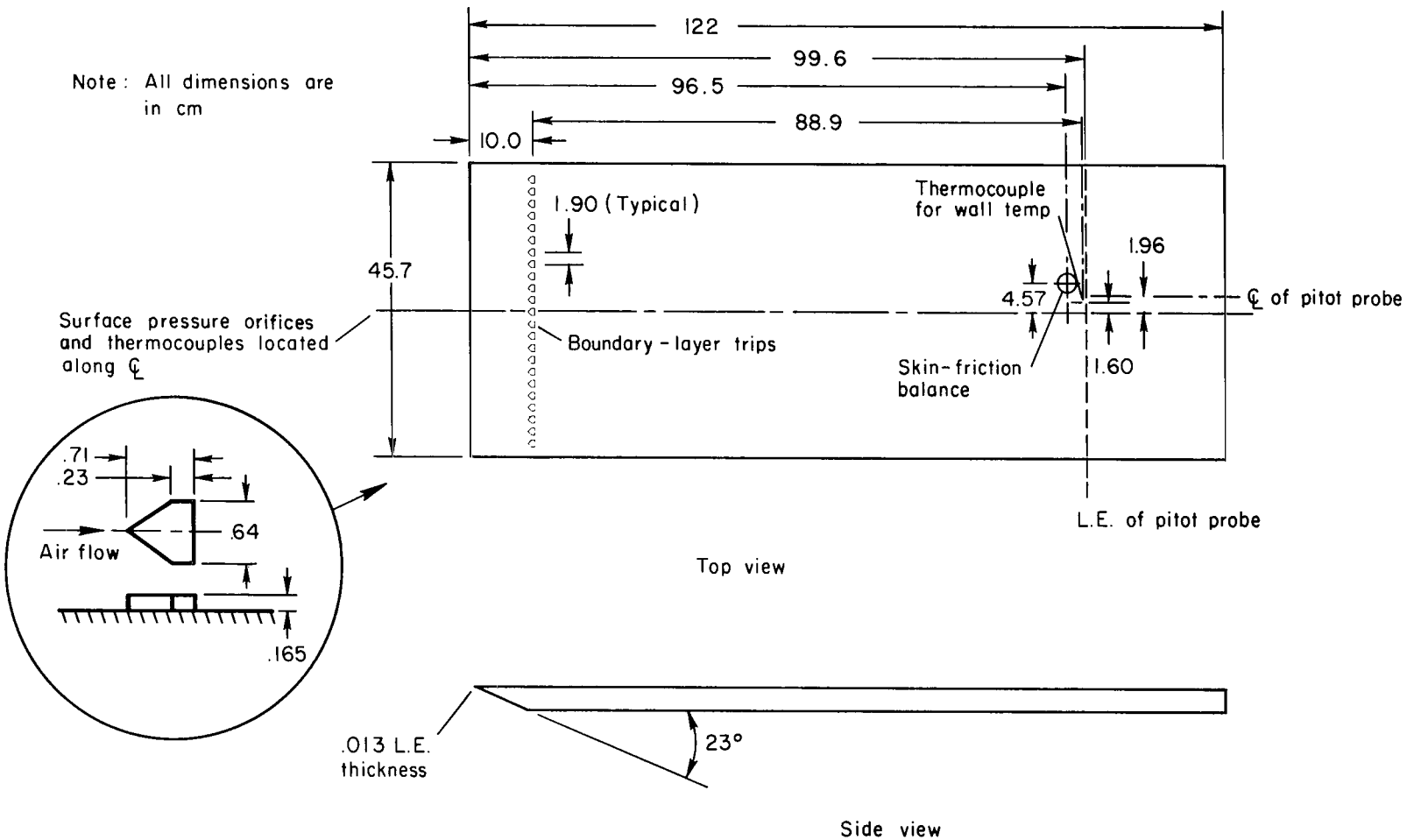

(b) Geometry.

Figure 1.– Concluded.

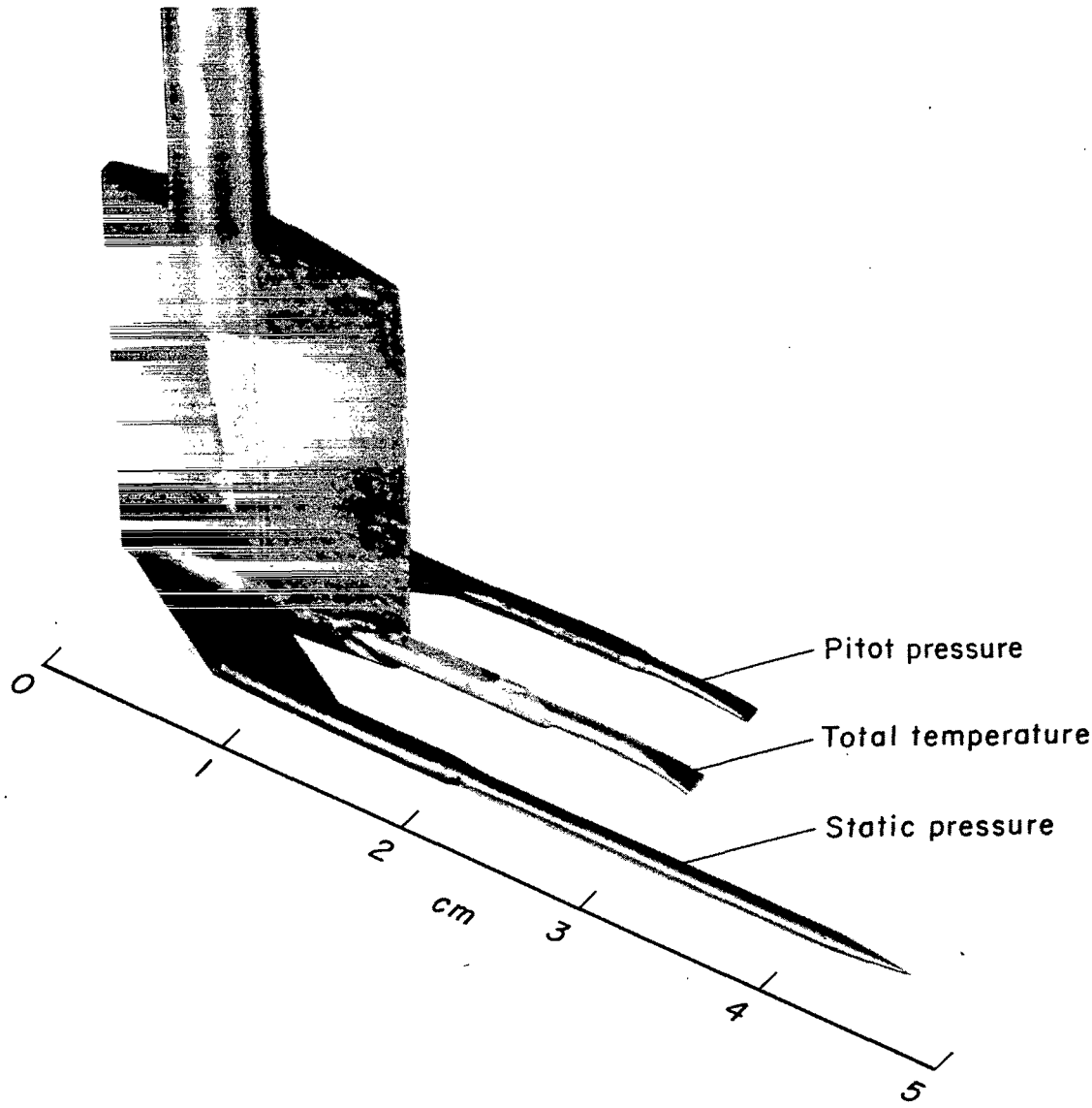

(a) Photograph.

Figure 2.– Boundary-layer survey complex.

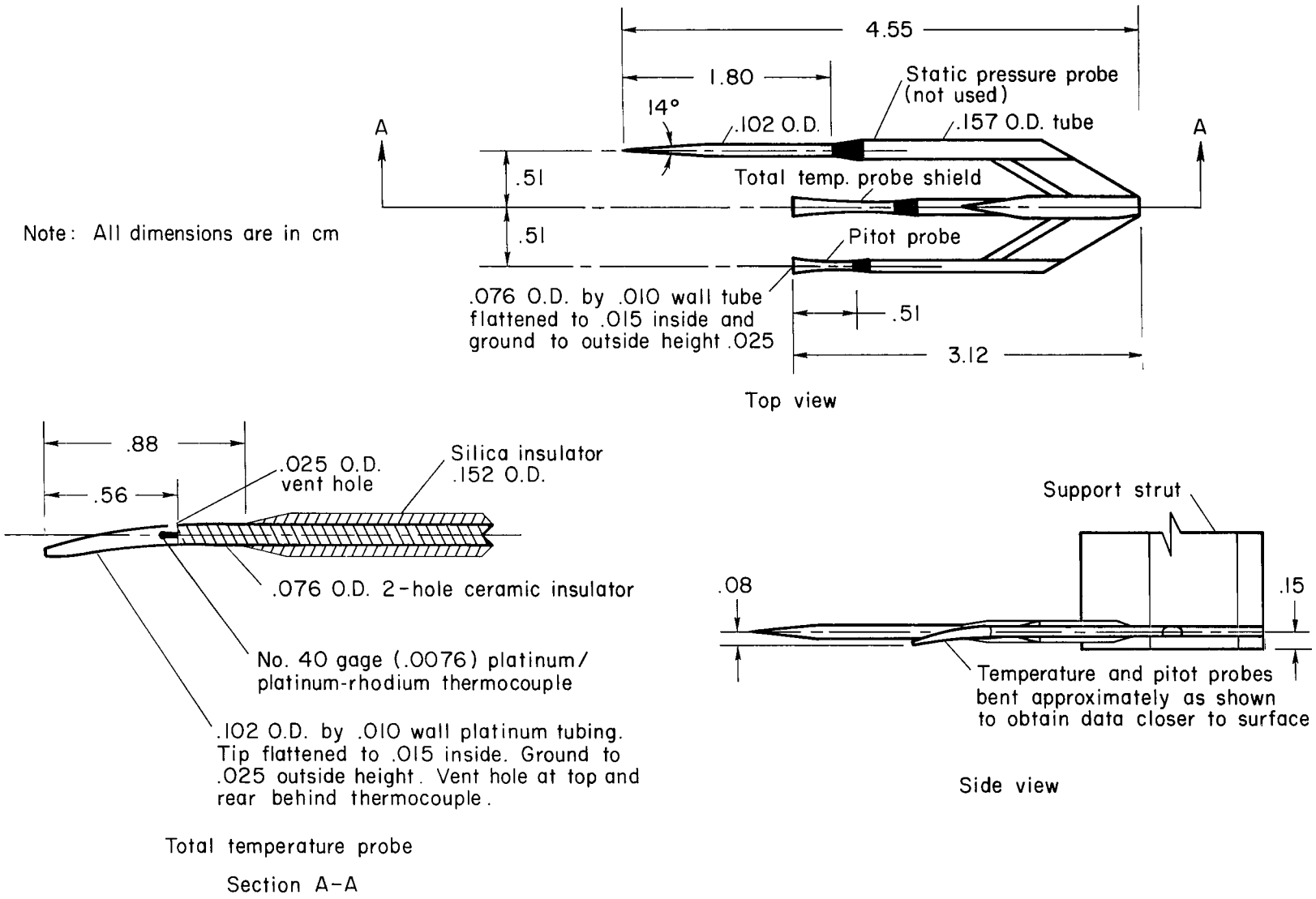

(b) Geometry.

Figure 2.- Concluded.

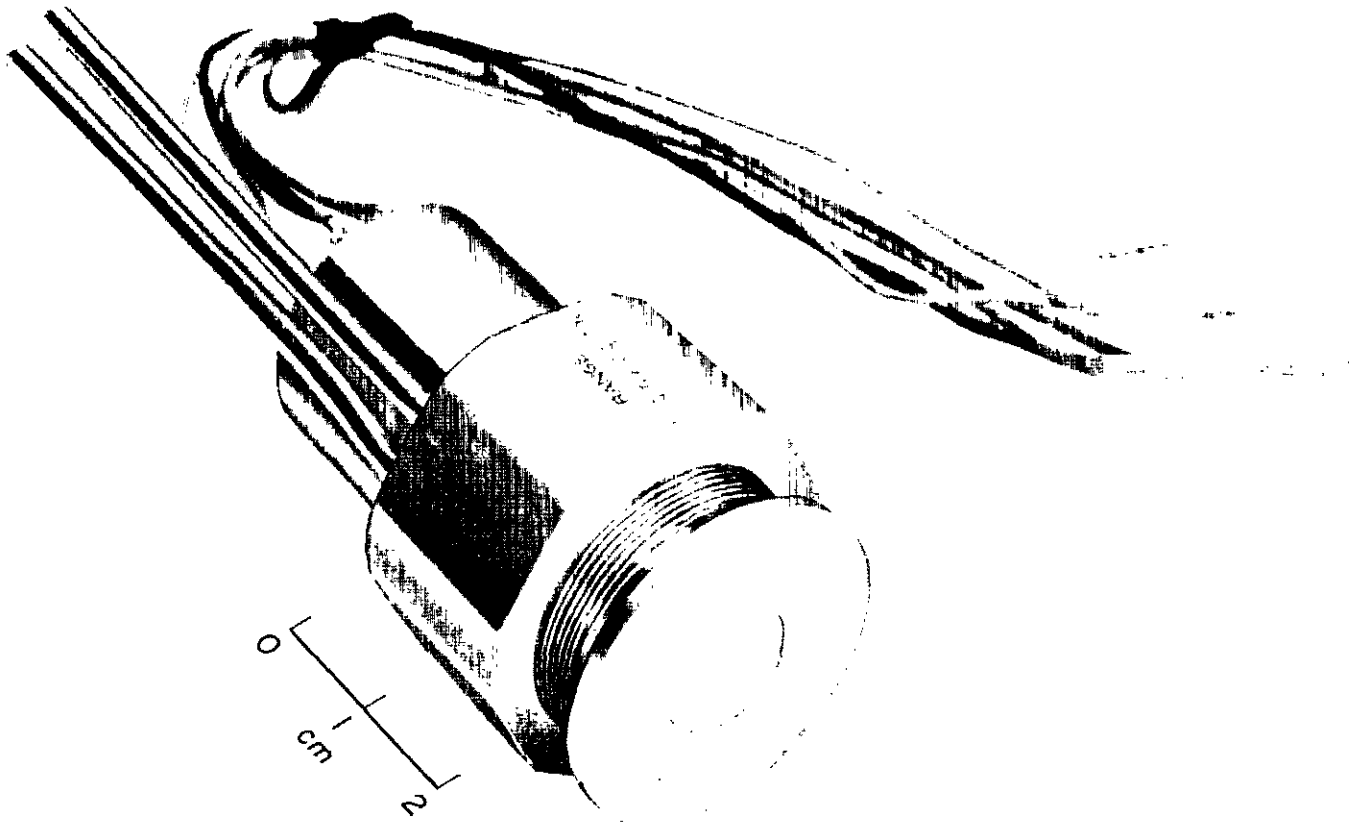

Figure 3.– Skin-friction balance.

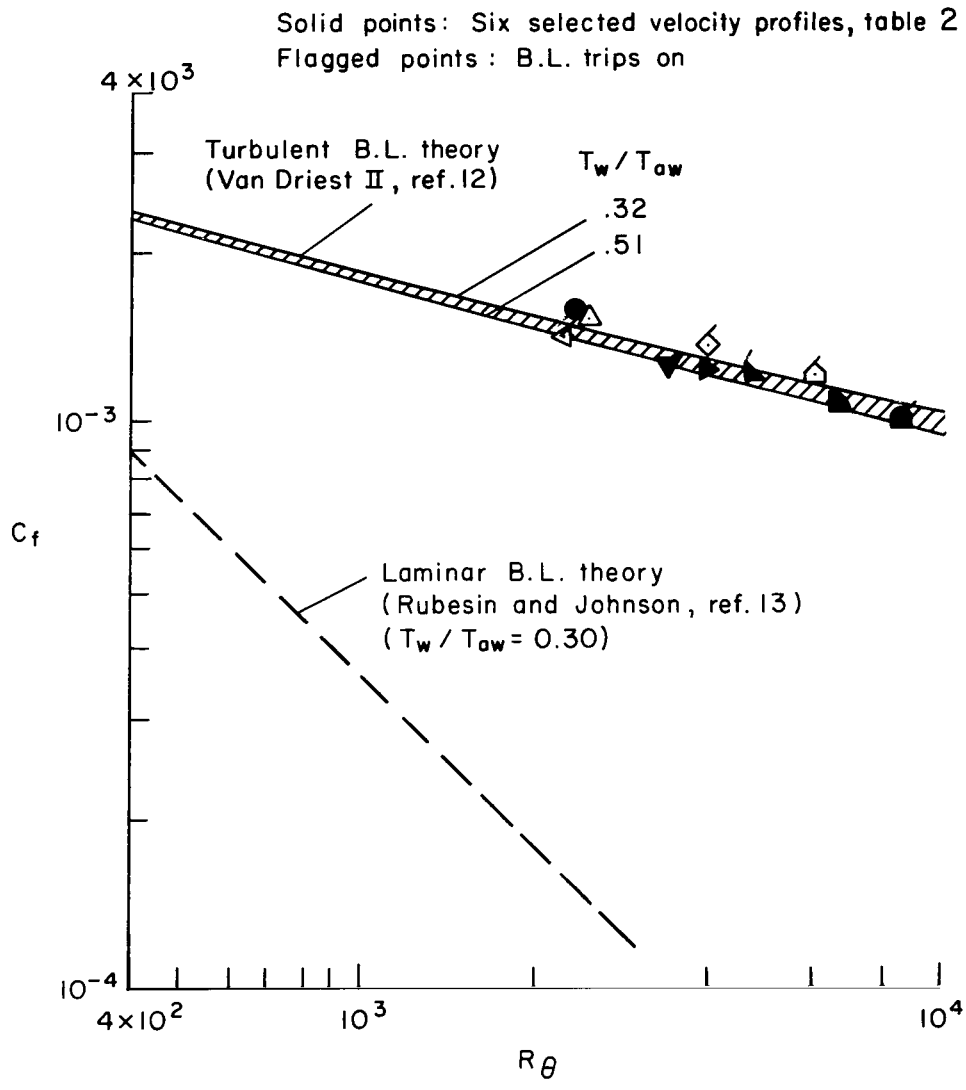

Figure 4.— Local skin-friction data (from ref. 2).

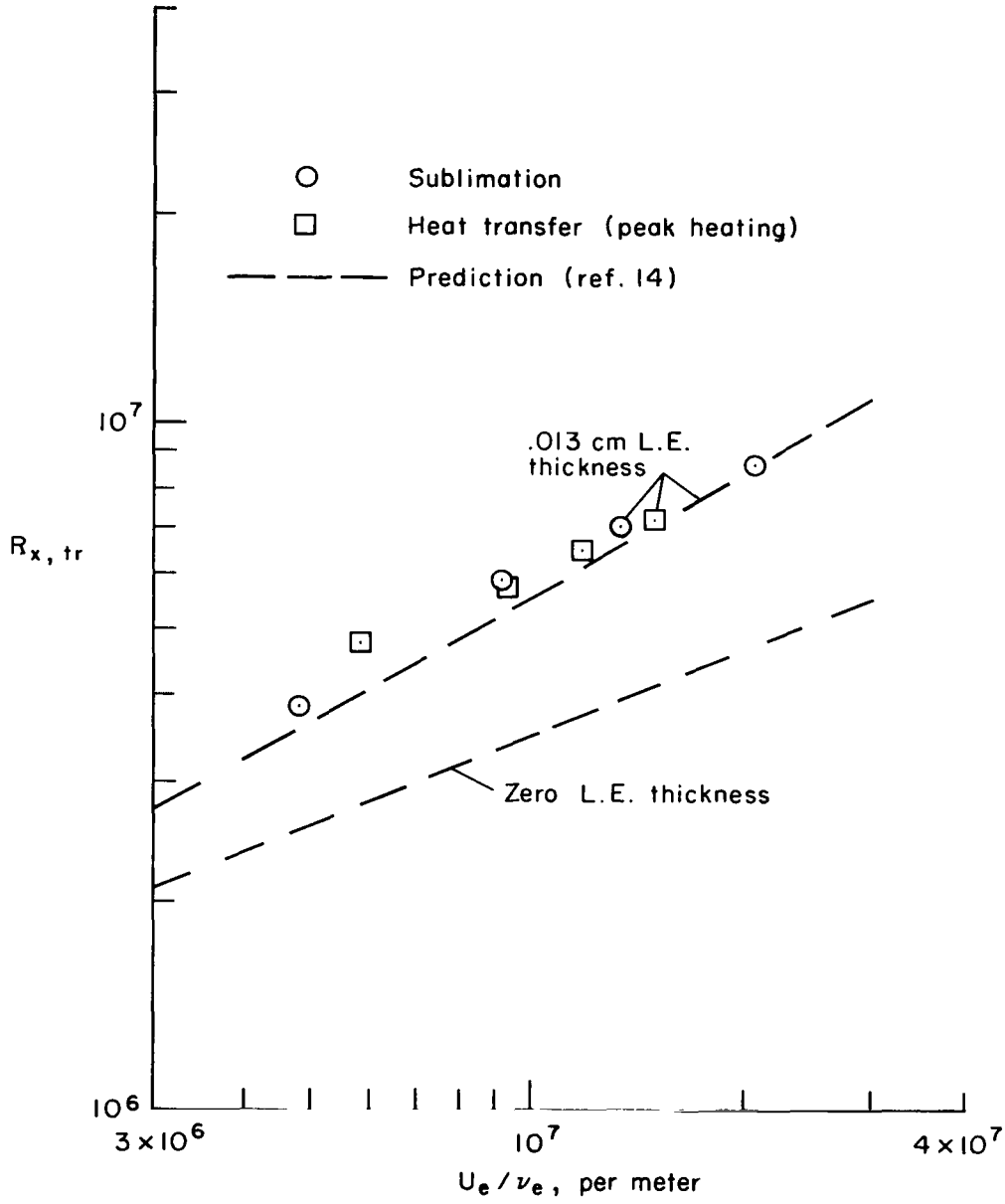

Figure 5.– Transition Reynolds numbers for end of transition.

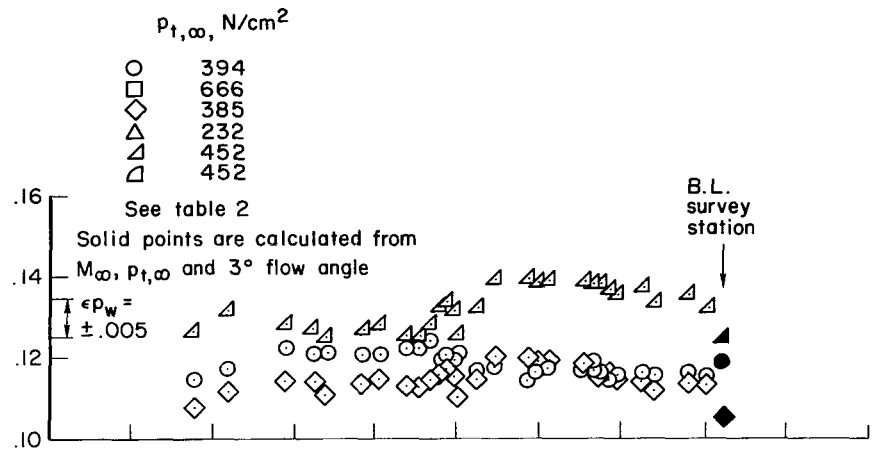

(a) Boundary-layer trips off.

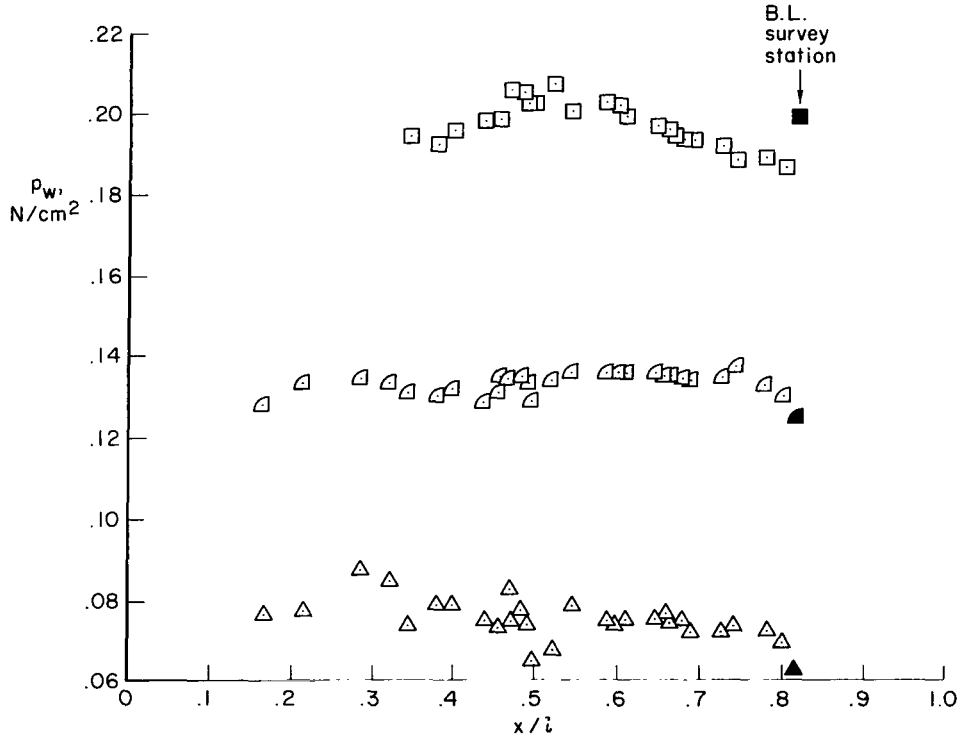

(b) Boundary-layer trips on.

Figure 6.– Surface-pressure distribution.

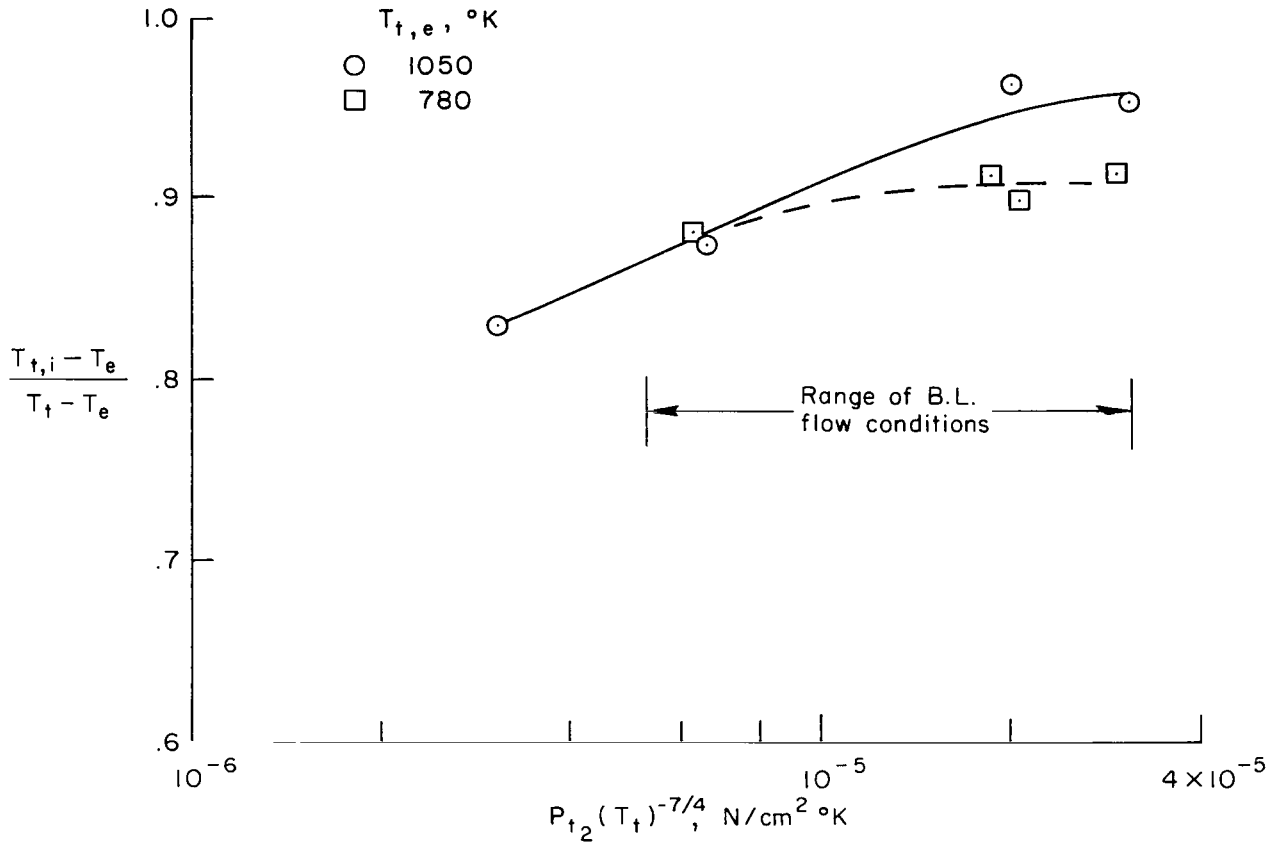

Figure 7.– Total temperature probe calibration.

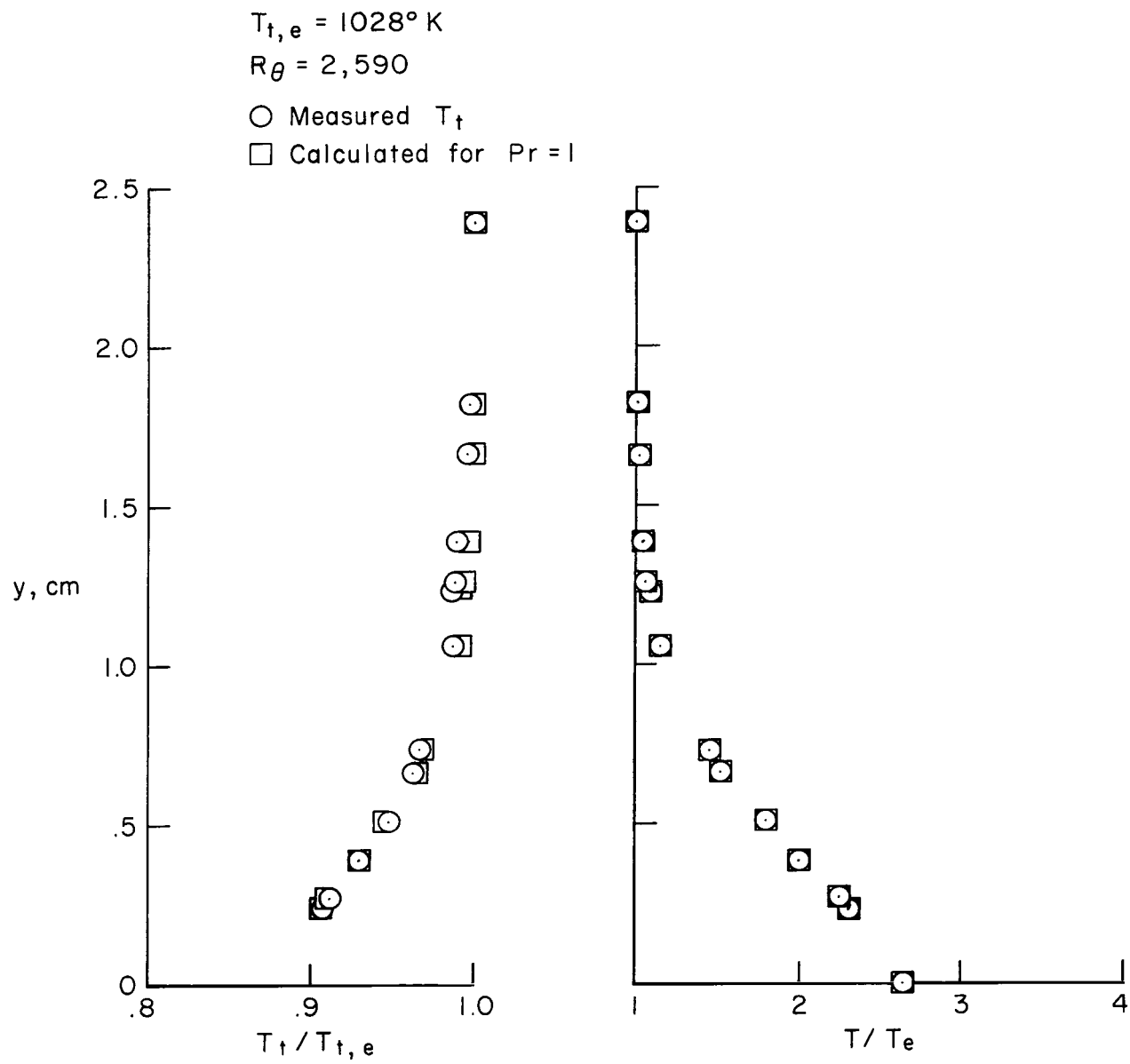

(a) Profile (a), table 2.

Figure 8.–Boundary-layer temperature profiles.

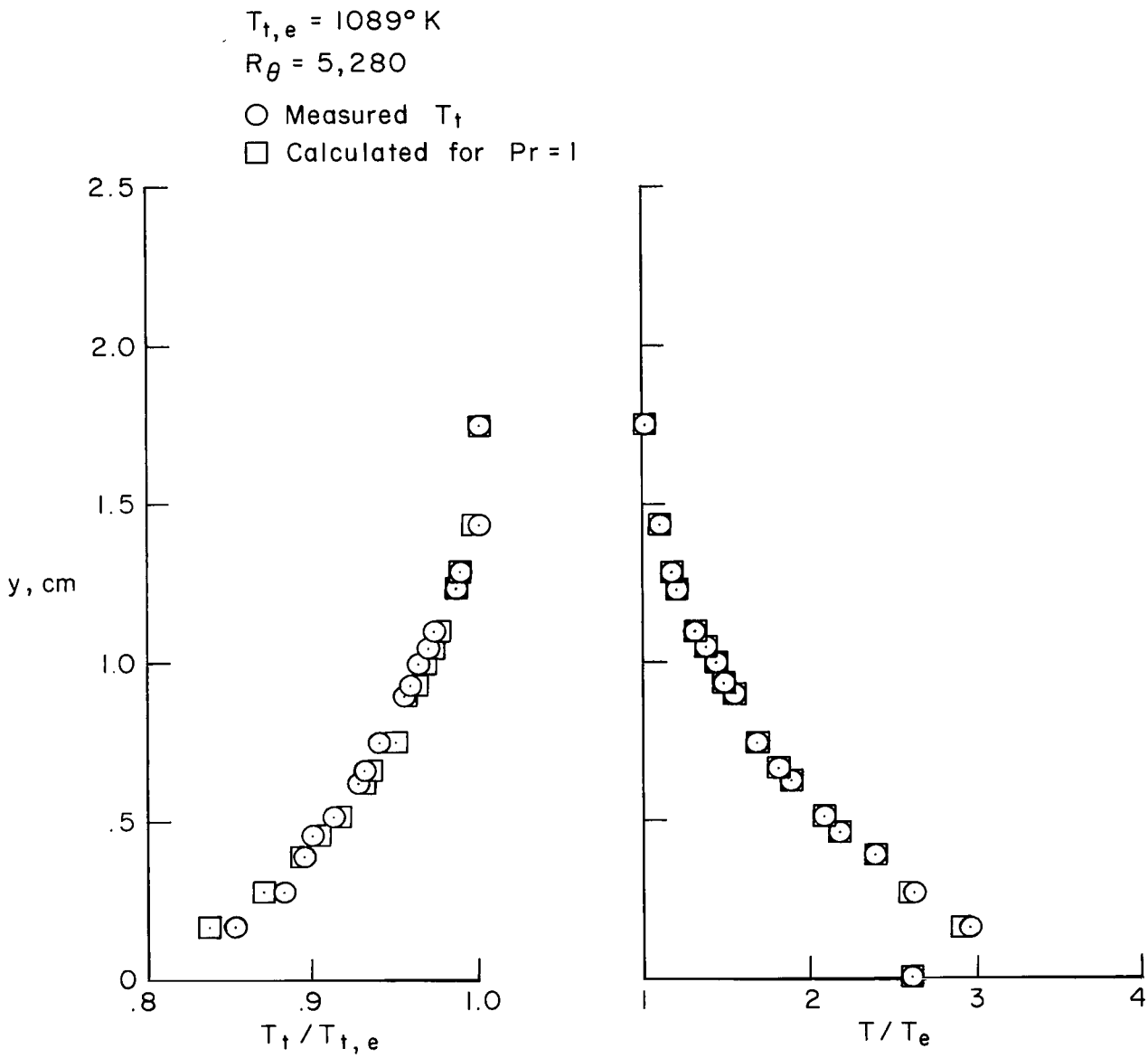

(b) Profile (b), table 2.

Figure 8.- Continued.

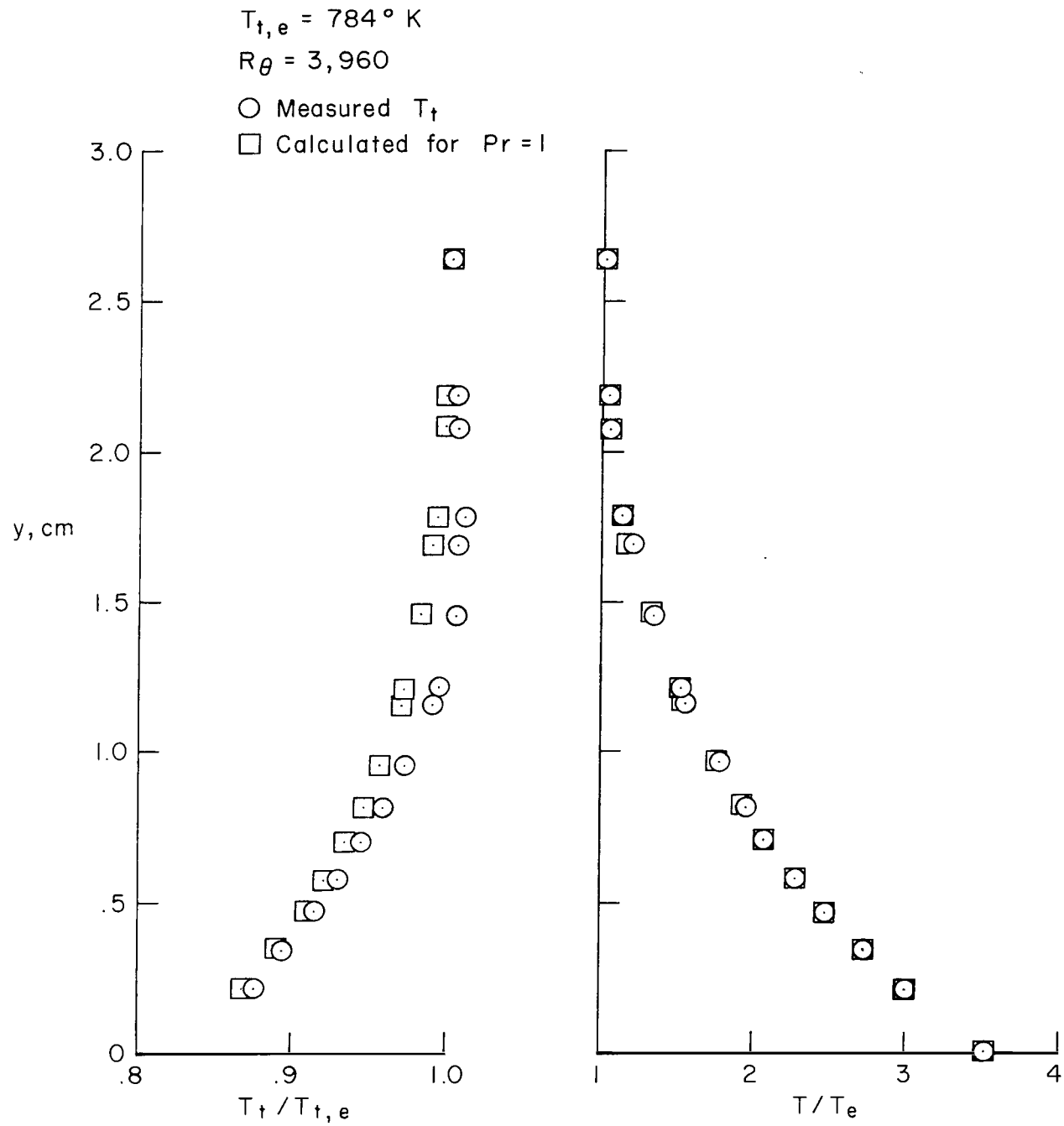

(c) Profile (d), table 2.

Figure 8.–Concluded.

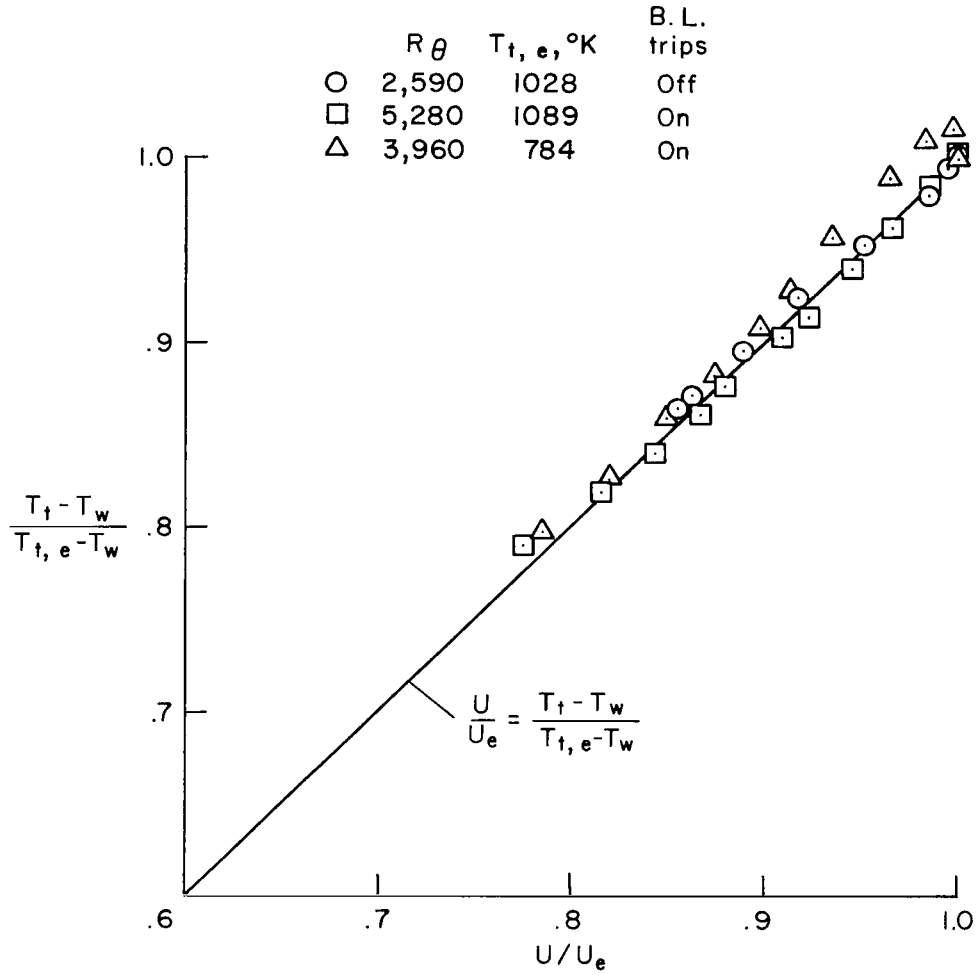

Figure 9.–Measured temperature-velocity profiles.

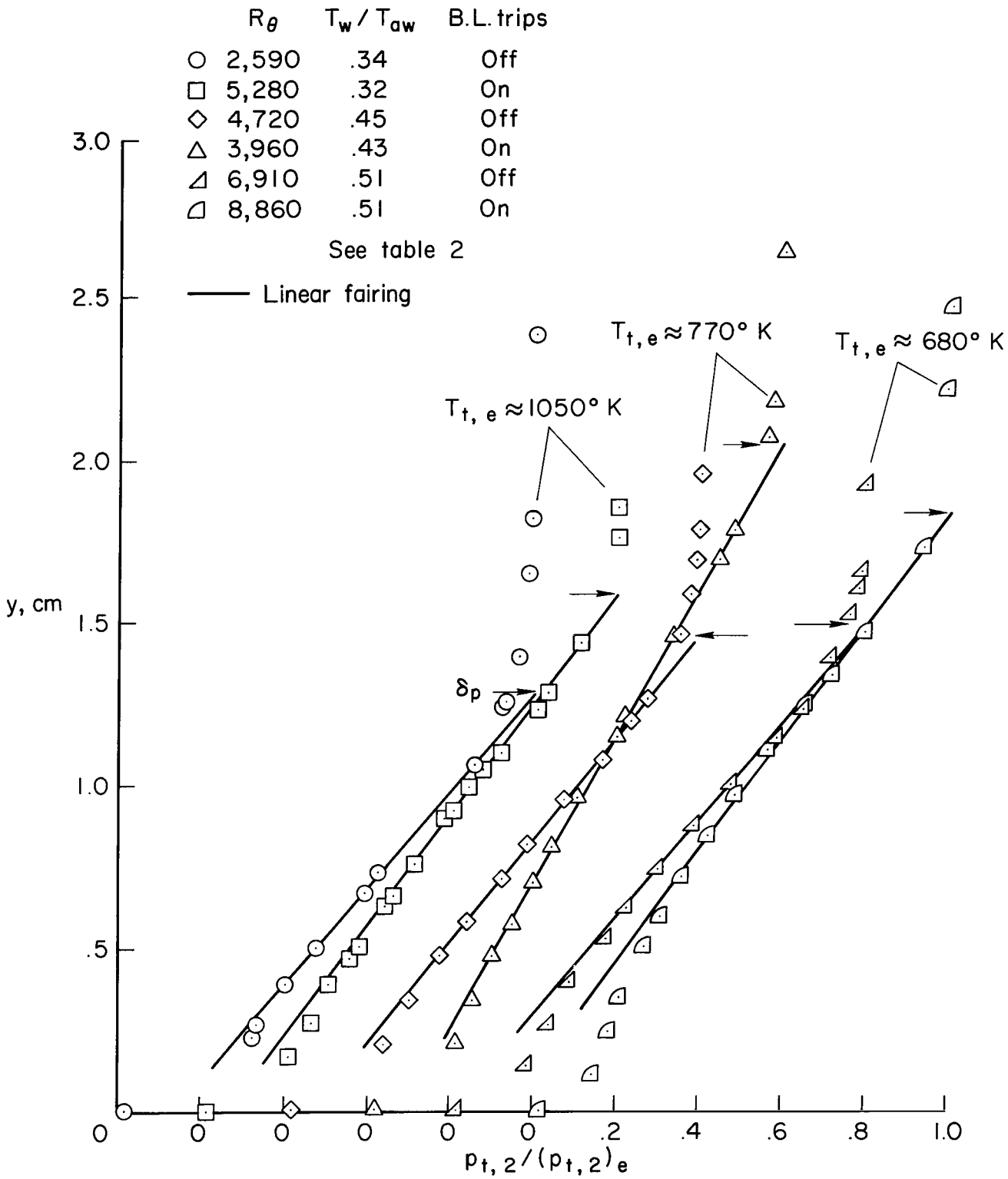

Figure 10.–Boundary-layer pitot-pressure profiles.

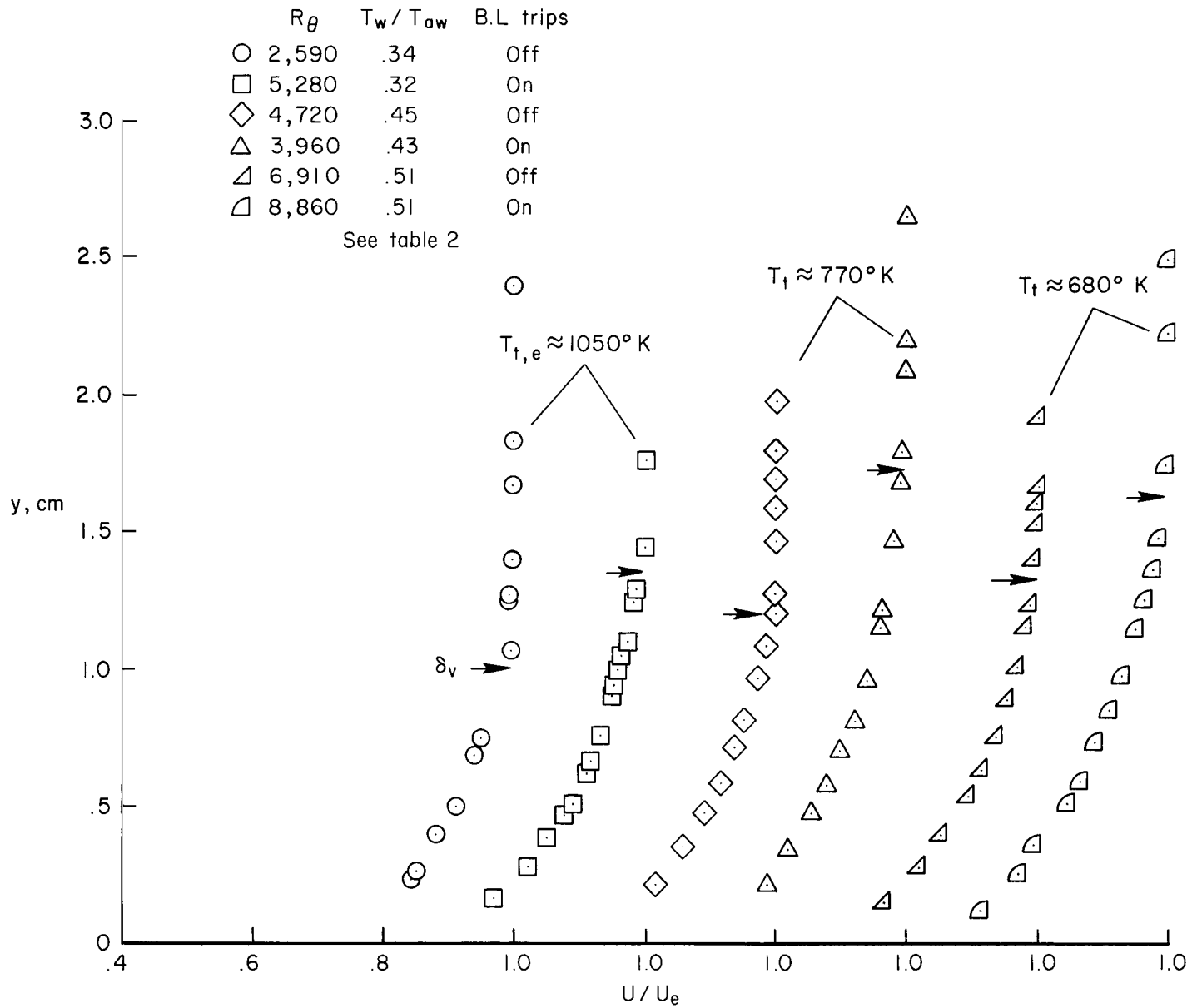

Figure 11.–Boundary-layer velocity profiles.

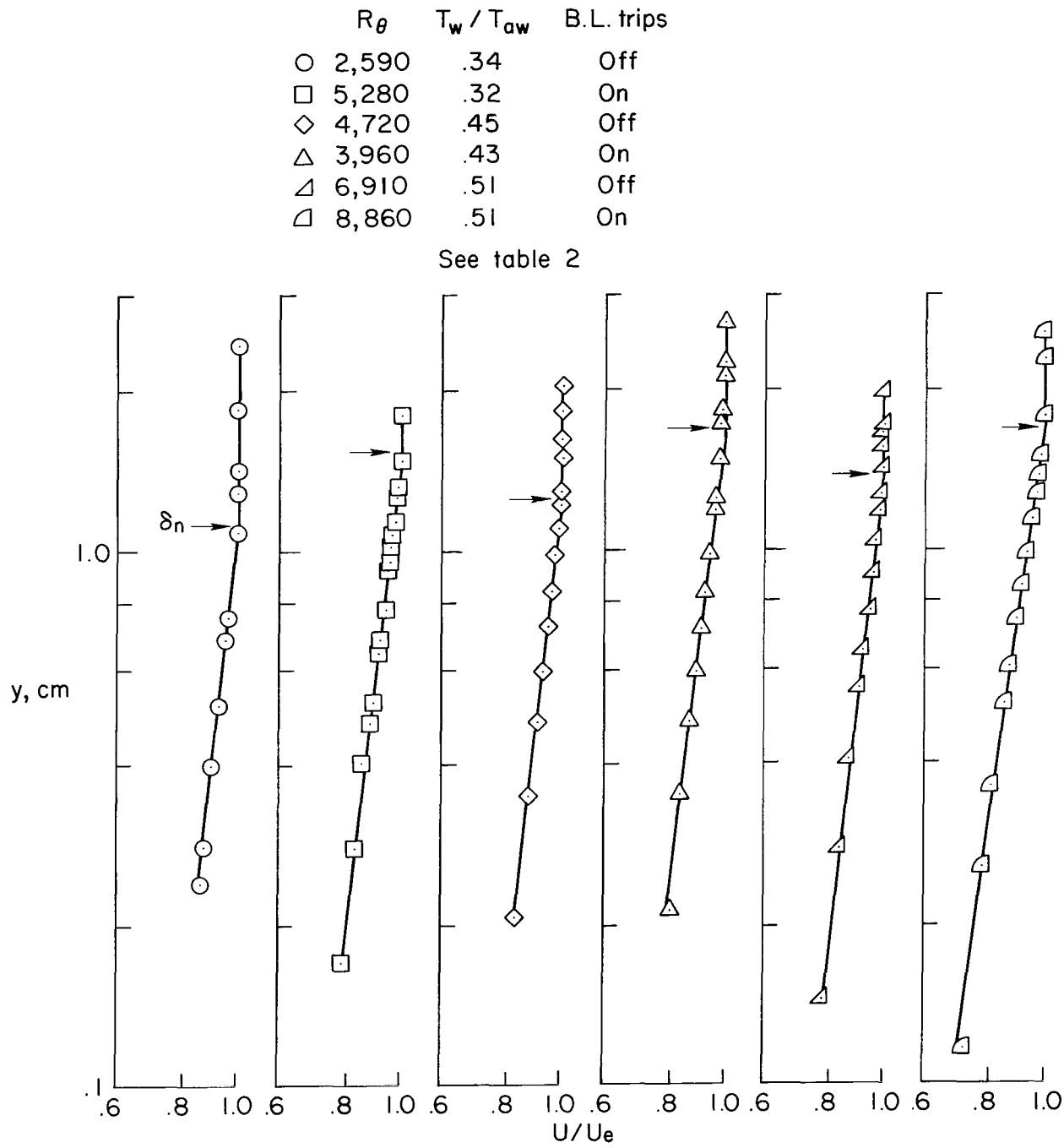

Figure 12.–Velocity-profile power-law plots.

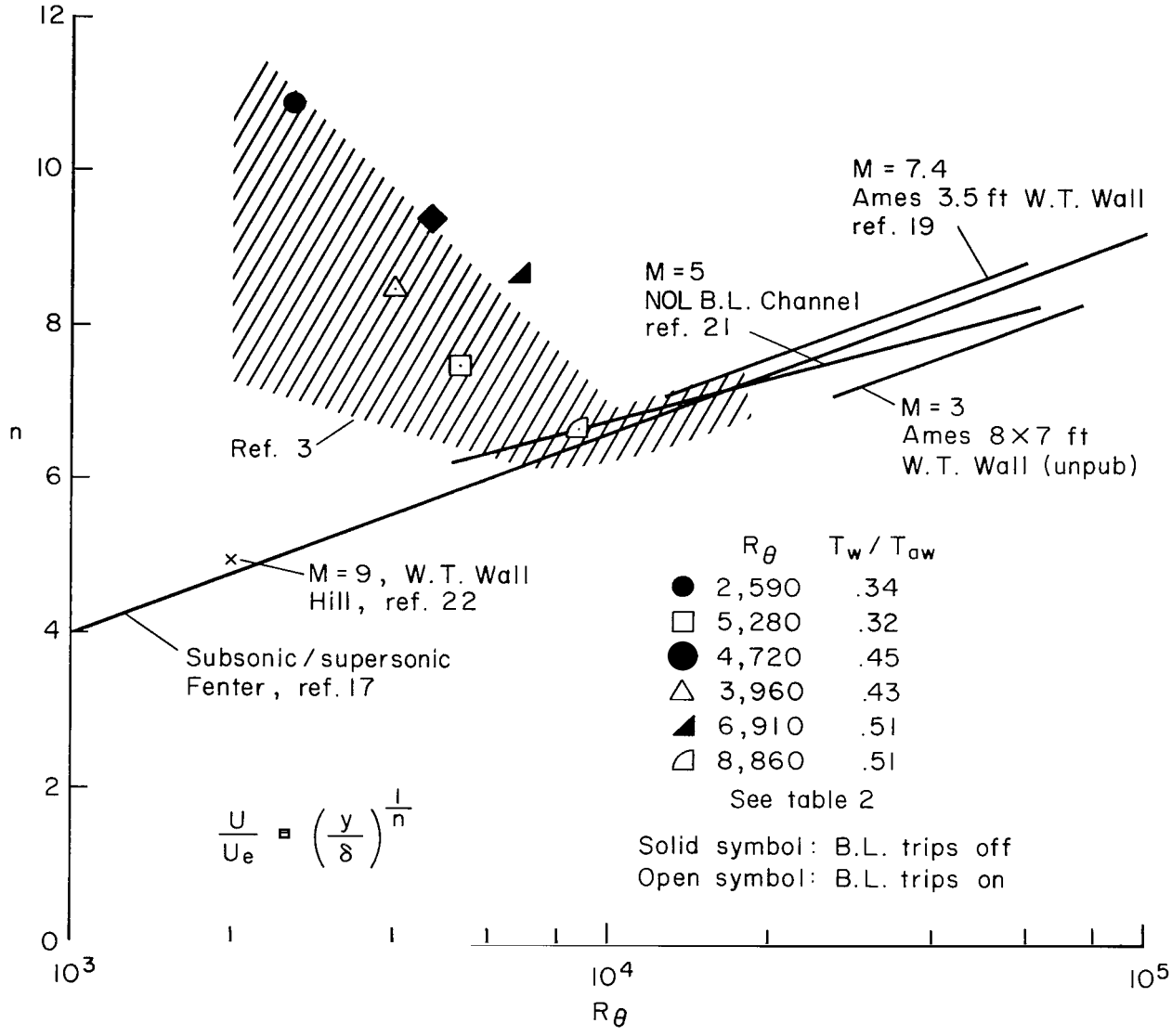

Figure 13.– Velocity-profile power-law exponent.

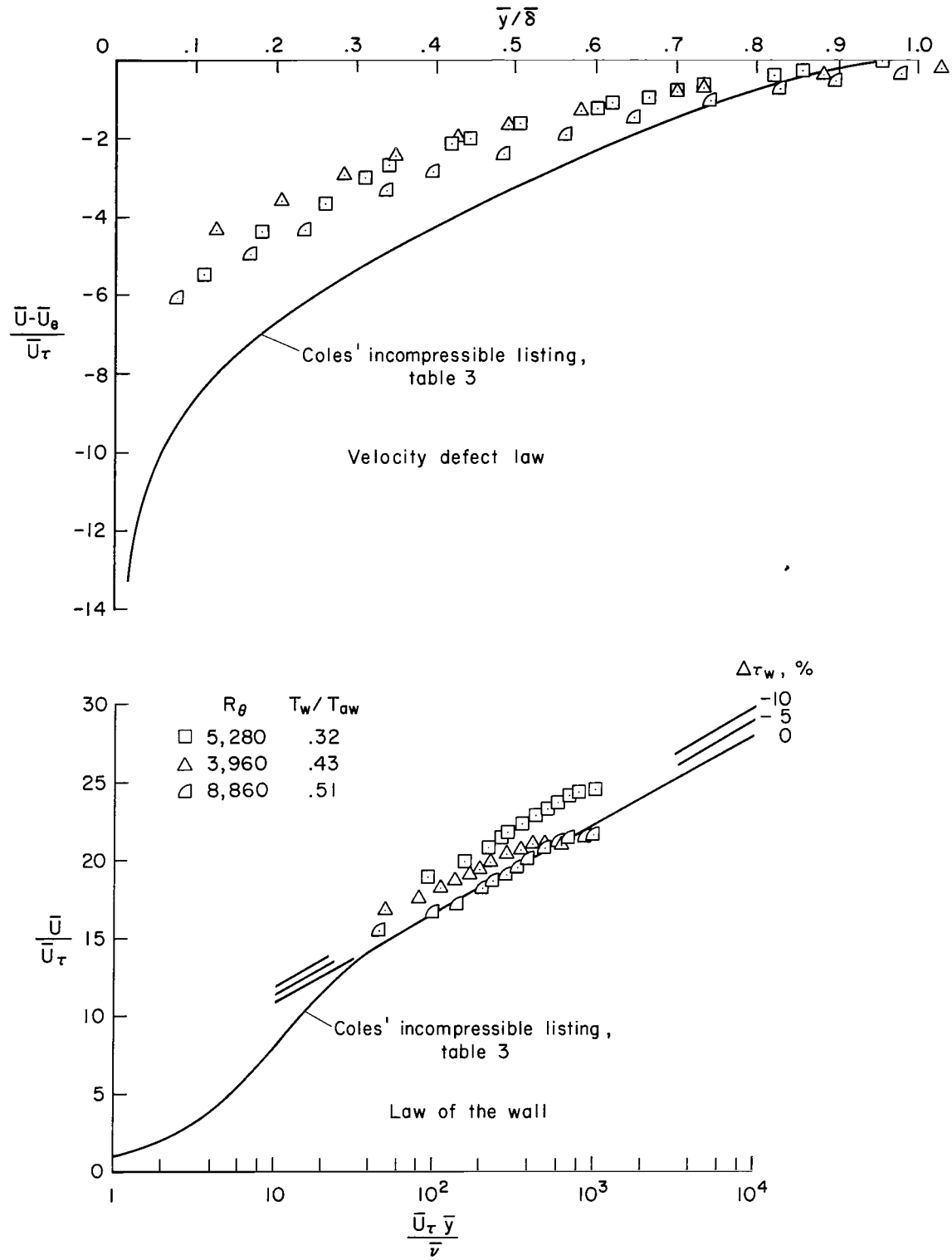

Figure 14.- Wall reference temperature transformation method (eqs. (1)-(4)); boundary-layer trips on.

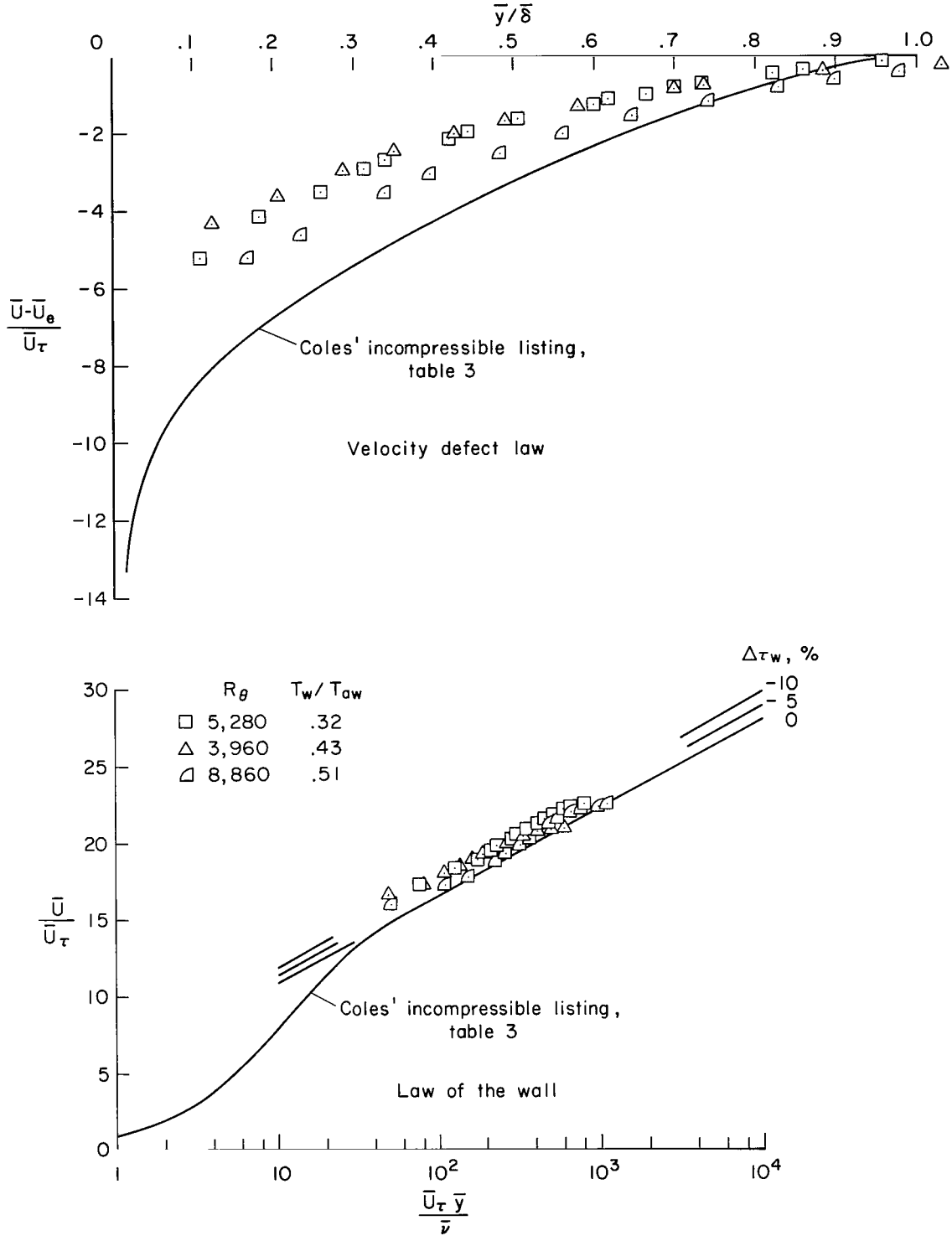

Figure 15.– T-prime reference temperature transformation method (eqs. (5)-(9)); boundary-layer trips on.

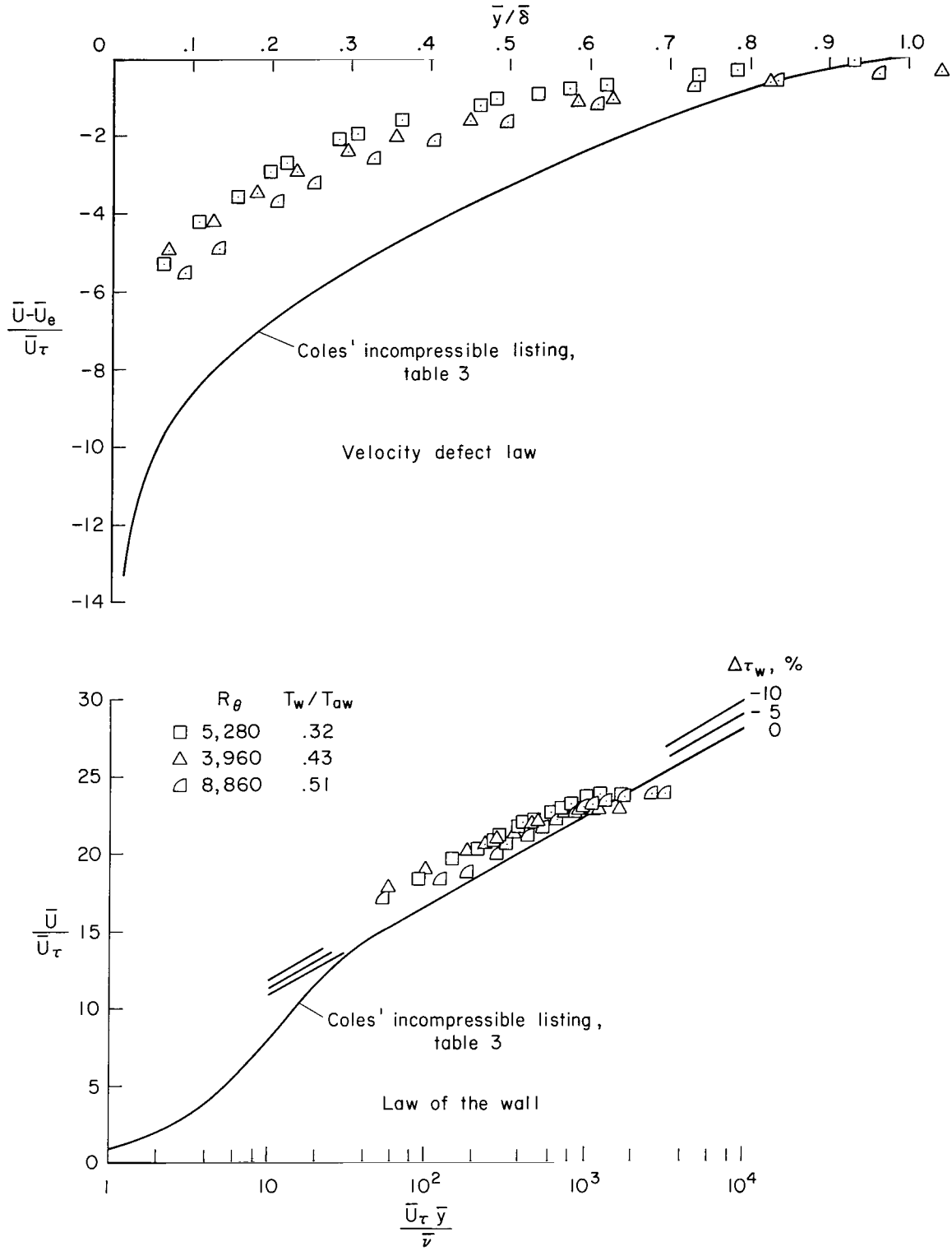

Figure 16.–Corresponding-stations transformation method of Coles (eqs. (10)-(17)); boundary-layer trips on.

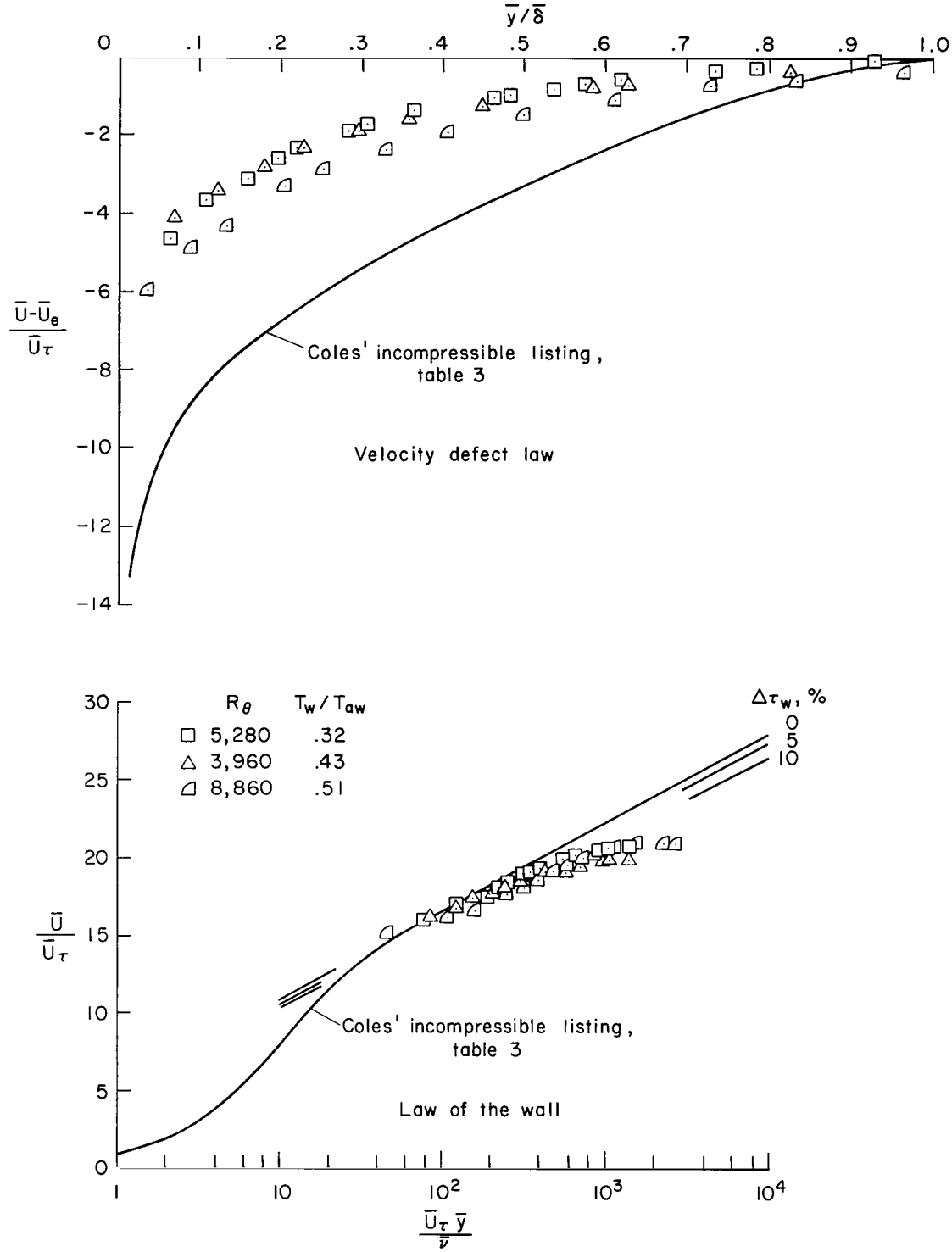

Figure 17.- Corresponding-stations transformation method of Baronti and Libby (eqs. (18)-(24)); boundary-layer trips on.

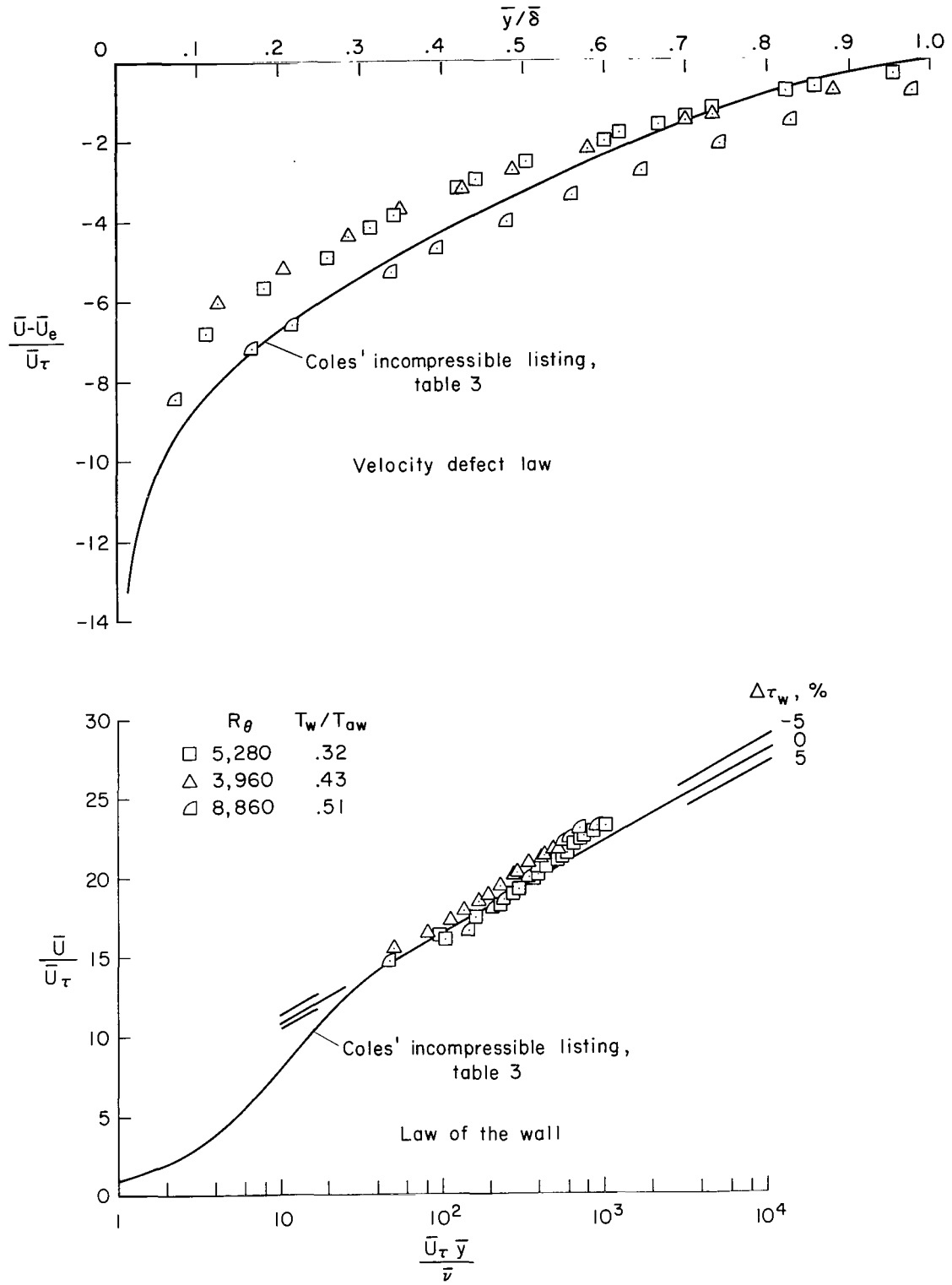

Figure 18.- Mixing-length transformation method of Van Driest (eqs. (25)-(30)); boundary-layer trips on.

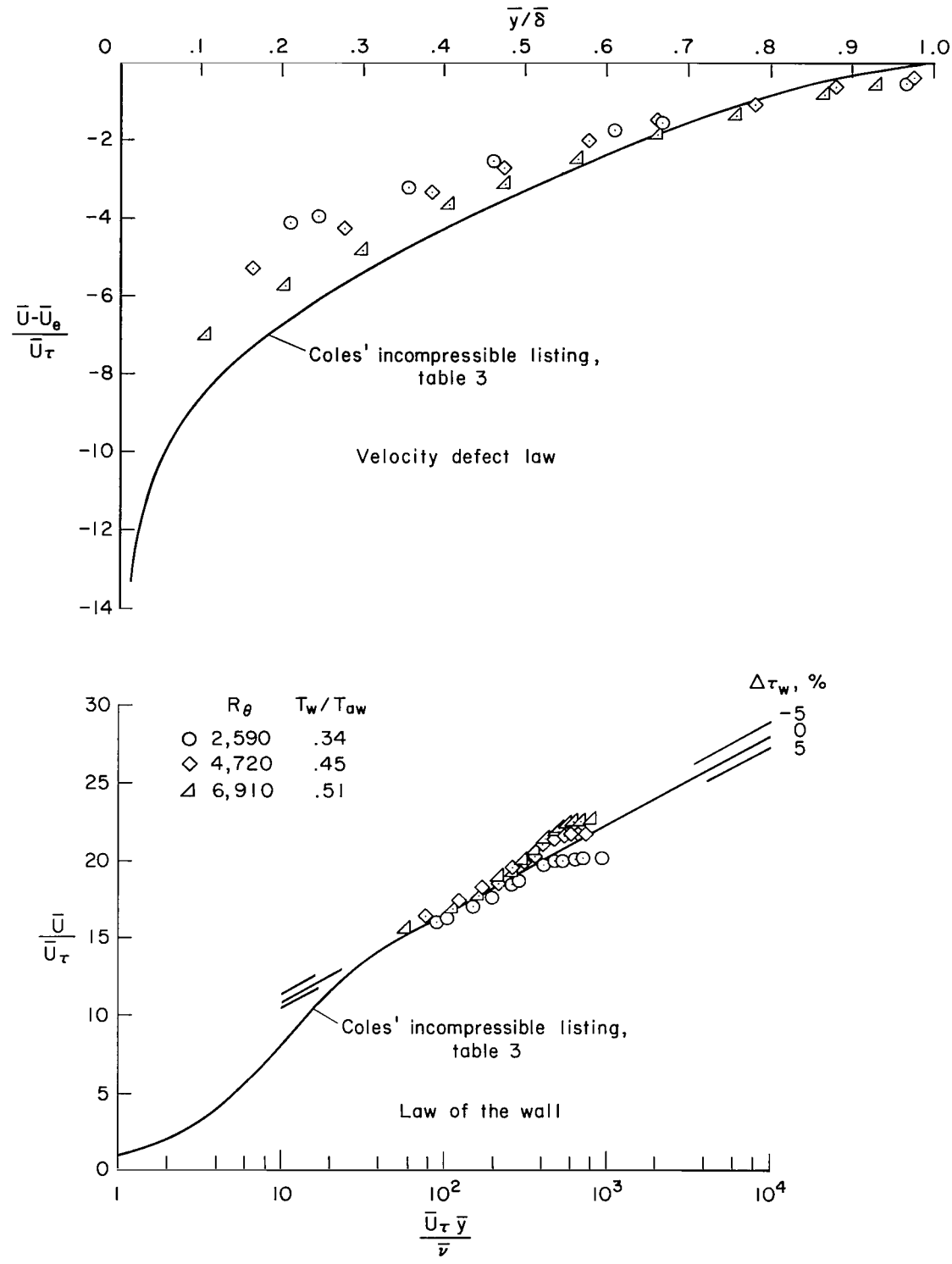

Figure 19.–Mixing-length transformation method of Van Driest; boundary-layer trips off.